PUBLISHER :

Address of Publisher
& Editor's Office :

GDAŃSK UNIVERSITY
OF TECHNOLOGY
Faculty
of Ocean Engineering
& Ship Technology

ul. Narutowicza 11/12
80-952 Gdańsk, POLAND
tel.: +48 58 347 17 93
fax : +48 58 341 47 12
e-mail : sekoce@pg.gda.pl

Account number :
BANK ZACHODNI WBK S.A.
I Oddział w Gdańsku
41 1090 1098 0000 0000 0901 5569

Editorial Staff :
Witold Kirkor Editor in Chief
e-mail : kirwik@interia.pl
Przemysław Wierzchowski Scientific Editor
e-mail : wierzche@xl.wp.pl
Maciej Pawłowski Editor for review matters
e-mail : mpawlow@pg.gda.pl
Tadeusz Borzęcki Editor for international relations
e-mail : tadbor@pg.gda.pl
Cezary Spigarski Computer Design
e-mail : biuro@oficynamorska.pl

Domestic price :
single issue : 20 zł

Prices for abroad :
single issue :
- in Europe EURO 15
- overseas US$ 20

ISSN 1233-2585

POLISH MARITIME RESEARCH

in internet

www.bg.pg.gda.pl/pmr.html

Index and abstracts
of the papers
1994 ÷ 2004

POLYTECHNICA GEDANENSIS
PATRIAE MARIQUE FIDELIS

POLISH MARITIME RESEARCH

No 2(44) 2005 Vol 12

CONTENTS

The papers published in this issue have been reviewed by :
Assoc.Prof. M. Dzida ; Prof. J. Kolenda
Prof. K. Rosochowicz ; Prof. Z. Starczewski
Prof. T. Szelangiewicz

Editorial

POLISH MARITIME RESEARCH is a scientific journal of worldwide circulation. The journal appears as a quarterly four times a year. The first issue of it was published in September 1994. Its main aim is to present original, innovative scientific ideas and Research & Development achievements in the field of :

Engineering, **Computing & Technology**, **Mechanical Engineering**,

which could find applications in the broad domain of maritime economy. Hence there are published papers which concern methods of the designing, manufacturing and operating processes of such technical objects and devices as : ships, port equipment, ocean engineering units, underwater vehicles and equipment as well as harbour facilities, with accounting for marine environment protection.
The Editors of POLISH MARITIME RESEARCH make also efforts to present problems dealing with education of engineers and scientific and teaching personnel. As a rule, the basic papers are supplemented by information on conferences , important scientific events as well as cooperation in carrying out international scientific research projects.

Editorial Board

Stability of free-floating ship

Part I

Maciej Pawłowski
Gdańsk University of Technology

ABSTRACT

Problem of calculation of righting arms of the free-floating ship, i.e. longitudinally balanced at any heel angle, was formulated. In such a case of particular interest for a ship in the damage condition, the righting arms are ambiguous as they depend on a way the heeling moment acts. Two cases were considered : when the heeling moment is parallel to the ship plane of symmetry, and the case when it performs the least work, i.e. when the moment is parallel to the main axis of ship waterplane. It was demonstrated that angular translations (heel and trim) are then the Euler angles associated with a relevant reference axis. Some cases of the incorrect defining and using of those angles in today design practice were indicated. The most important features of the curve of righting arms of free-floating ship were demonstrated.

Keywords : stability, free floating ship

INTRODUCTION

Rules of the classification societies require the intact ship stability to be investigated for the ship floating at even keel. The rules, however, do not clearly state how to calculate the damaged ship stability, which often leads to large discrepances in obtained results.

For the undamaged ship it is practically meaningless whether the stability calculations are performed for the ship having a fixed trim, constant in function of the heeling angle, or for the free-floating ship which changes its trim depending on its longitudinal equilibrium state. This is due to a small asymmetry of the ship relative to its midship section plane. However for the damaged ship the problem is important as it significantly influences the course of the righting arm curve for the heeeling angles greater than the entrance angle of the deck into water (Fig.1). The righting arm is understood here as the distance between the action line of buoyancy force and that of gravity force, occurring in still water, at a given heeling angle.

The influence of calculation assumptions is especially important in the case of flooding compartments far off the midship, which is understable due to the then occurring high asymmetry and a small entrance angle of the deck into water. Moreover the influence very strongly increases along with the ratio L/B decreasing. Hence it is greater for catamarans and SWATH units. The differences between righting arms may even reach a few hundred percent. For this reason the regulations should clearly define a way of carrying out calculations : whether at a fixed or free trim. It should be remembered that the final aim of stability calculations is to determine an expected final state of a considered ship under action of disturbing moments – and as a result – to correctly assess stability safety of the ship.

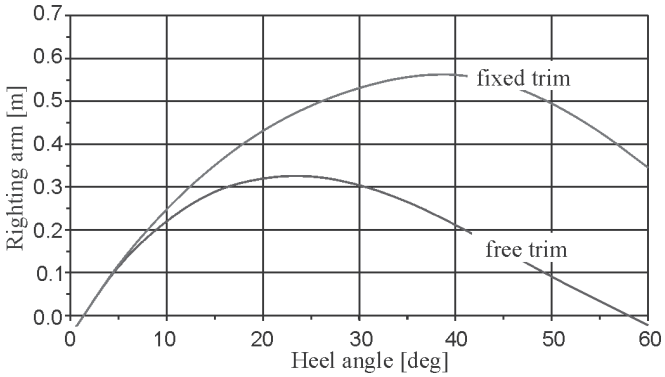

Fig. 1. *Righting arm curves for a free-floating damaged ship and that having a fixed trim [1]*

It is obvious that the routine stability calculations should be performed for a free-floating ship. However in such commonly accepted case the problem of correctly understood ship heel angle arises because then it is an ambiguous notion, which is manifested in existing various definitions of that angle. Most often the heel angle is assumed to be the slope angle of water-level trace line on the frame planes, further marked φ, or the slope angle of the baseplane (BP) relative to water-level , further marked α. The first of the angles is loosely associated with correctly defined ship heel angle, whereas the second is the heel angle of the ship having minimum righting arms.

HEEL ANGLE OF FREE-FLOATING SHIP

The problem of correct defining the heel angle of the free-floating ship has been recently solved [2÷4]. Namely, the ship heel angle, further marked ϕ, is understood as the angle rota-

tion of the ship plane of symmetry (PS) around the intersection line of water surface and PS, i.e. the angle of rotation around the water-level trace line on PS, in other words – this is the inclination angle of PS from the vertical. At the same time the angle is equal to the slope angle of the axis *y* relative to water surface. The definition stems from the assumption that the ship heels under action of the heeling moment of fixed direction in space, and parallel to PS. If the ship floats freely it heels in such a way as to be logitudinally balanced all the time. It means that the direction of the righting moment is fixed in space[1)] and the same applies to the heeling moment. The conclusion immediately follows that the curve of buoyancy centres is then exactly flat and situated on the *rotation plane* perpendicular to the heeling moment vector, and containing the ship centre of gravity.

A necessity to define the heel angle of free-floating ship is usually not felt – many surveyors and designers are just surprised that any problem of this kind exists at all. Hence various definitions of the angle in question have been still assumed, which obviously results in ambiguity of calculation and makes it not possible to compare different computer softwares.

HISTORICAL OUTLINE

Why a body floats in a liquid has been known already in antiquity since the times of Archimedes. However in which way to assess and investigate stability of floating bodies has been recognized only after discovery of the Newtonian laws. In 1746 Bouguer introduced the notion of metacentrum and metacentric height considered as a measure of initial stability. In 1749 Euler introduced a formula for metacentric radius, and a theorem for equi-volume waterplanes. In 1796 Atwood published a method for calculation of the righting arm at a given heel angle [5]. Nonetheless for over a hundred years only the initial metacentric height GM was used to assess ship stability. Only the ship stability accidents at the end of 19th century revealed importance of the freeboard and necessity of applying the curve of righting arms in assessing stability of ships.

The metacentric height, which is not an unimportant index of stability, does not make it possible to directly assess either a range of the curve of righting arms nor on a value of the maximum righting arm. Here it is worth mentioning the widely described case of sinking the HMS *Captain* in 1870, whose metacetric height GM = 0.79 m [6]. The ship capsized during a storm in the Bay of Biscay, whereas the accompanying battleship *Monarch* of a similar size and characteristics survived unharmed despite having its metacentric height GM = 0.73 m, i.e. smaller than that of the first ship. The fact was very surprising for the then naval architects. It is very easy to explain the accident if one observes that the freeboards of the two ships much differred to each other : the *Captain* had the freeboard F = 1.98 m and the *Monarch* - F = 4.27 m. As a result, despite the smaller metacentric height of the *Monarch*, its curve of righting arms was of much better parameters than that of the *Captain*, whose GZmax = 0.55 m instead of 0.25 m, $\phi_{max} = 40$ deg instead of 19 deg, and the stability range angle $\phi_v = 70$ deg instead of 54 deg.

The *Captain's* accident has finally proved that the metacentric height is an insufficient measure of safety against capsizing and it has made it necessary to examine ship's stability also at large heel angles. As a result, at the end of the 19th century the curves of righting arms, called the *Reed's* curves in memory of their propagator, began to be used for the ship stability assessment. The first stability criteria, given by Rahola [7], appeared as late as in 1939. The well-documented recommendations dealing with a minimum size of the curve of righting arms have been elaborated on the basis of the analysis of the curves of righting arms of both for capsized ships and stable ones. At the end of the 1960s those criteria were adopted by IMCO (Intergovernmental Maritime Consultative Organization, presently IMO (International Maritime Organization), and they have been valid until now [8].

Though the curve of righting arms has been applied to assess stability of intact ships, stability of damaged ships has been further controlled by means of the metacentric height and freeboard. In the SOLAS conventions including the last one of 1974 the residual freeboard of as low as only 3 inches and the metacentric height of 2 inches have been assumed permissible. With such parameters the curves of righting arms usually show marginal values. A change took place as late as in 1990 when criteria for the curve of righting arms were introduced for damaged ships, in the form of the SOLAS 90 criteria [9]. However it is worth remembering that the criteria have not represented any important progress as they resulted from an administrative decision. Therefore they have only an alleged, but not real, relation to actual safety of a ship in damage condition. A breakthrough in that regard has happened during the last six years [10,11].

FORMULATION OF THE PROBLEM

Almost all of the commonly known calculation methods of the curve of righting arms concern the ship floating on even keel. This means indirectly that the buoyancy centre is assumed not to translate longitudinally during ship's heeling. It has been no necessity to consider earlier a different situation as the calculations dealt only with intact ships for which the assumption has been well satisfied. However the fact cannot be neglected any longer in the situations when the buoyancy centre translates longitudinally due to an asymmetrical distribution of buoyancy relative to the plane of rotation, as in the case of semi-submersible platforms arbitrarily orientated relative to wind direction, ships of low L/B ratio, or ships in damage conditions, and then the calculations should be carried out for a free-floating object. Determination of the curve of righting arms becomes in such cases ambiguous and the problem must be defined. Especially the way in which the righting moment acts should be defined.

It should be said that angular motions of a free-floating object are not considered in the basic ship theory as this is a 3-D motion. And, such motion is spatial and requiring good spatial imagination. For this reason as well as for making calculations easier the vectorial calculus is applied in this paper.

Calculations of the righting arms curve for free-floating ship is carried out under the following assumptions :

a) ***a pure heeling moment is statically exerted on the ship***. It means that ship inclinations are equi-volumetric and the horizontal position of the ship gravity centre remains constant (the moment cannot induce any translational motion hence change location of ship gravity centre on the sea level)

b) ***the heeling moment vector is strictly horizontal***. If this is not the case a vertical component of the moment, able to rotate the ship around its vertical axis, will exist

c) ***the heeling moment direction is fixed in space and parallel to PS***. As the moment is simultaneously parallel to the water-plane hence it is also parallel to the trace line of water on PS. Therefore the intersection edge of PS and the water-plane is also fixed in space. The edge determines orientation of the ship at the sea level as well it defines the direction of the heeling moment [2)]

d) ***the ship is in static equilibrium***, i.e. the sum of forces and moments acting on it equals zero. Hence ship's weight is equal to its buoyancy, and the statically applied heeling mo-

ment is balanced by the righting moment of the same direction and opposite sense

e) ***the righting moment is formed by the couple of forces*** : i.e. the gravity force applied in the ship's centre of gravity and the buoyancy force applied in the ship's centre of buoyancy – the forces are equal and of opposite sense to each other. The moment's vector is horizontally directed, perpendicular to the vertical plane determined by the gravity force and buoyancy force.

From those assumptions some consequences follow :

- ⇨ As in the state of equilibrium directions of the moments are the same the centre of buoyancy must be situated on the plane perpendicular to the direction of action of the heeling moment (i.e. on the rotation plane), and on which the centre of gravity is located. As the direction of the heeling moment action is, under the assumption, fixed in space, hence the rotation plane is also fixed in space. The versor perpendicular to the rotation plane, further marked ***e***, is hence constant and stands for *the rotation axis*.
- ⇨ For ship heels at a fixed trim the centre of buoyancy need not to be located on the rotation plane, therefore the moment acting on the ship has not a constant direction at the horizontal plane.
- ⇨ The rotation plane is vertical, motionless in space, perpendicular to the direction of the moment action (trace of water on PS), and passing through the ship gravity centre G motionless at the horizontal plane.
- ⇨ It is the rotation plane about which the buoyancy centre of free-floating ship moves. Hence the curve of buoyancy centres is strictly flat in space. For ship heels at a fixed trim the curve of buoyancy centres is the projection of the spatial curve onto the rotation plane.
- ⇨ The trace of water on PS determines the direction of the heeling moment. The ship heel angle ϕ is the rotation of PS around the trace of water on PS, i.e. the deflection angle of PS from the vertical. As Oy-axis is perpendicular to PS the angle ϕ is simultaneously the slope angle of that axis against the water-level. The angle ϕ can be interpreted as the rotation angle of Oy-axis around the trace of water on PS, in the rotation plane.
- ⇨ In order the ship to be balanced at any heel angle ϕ it has also to rotate around the versor normal to PS, i.e. the Oy-axis, in such a way as to bring the centre of buoyancy on the rotation plane (Fig. 2). The ship rotation angle in PS, further marked θ, is called the trim angle – this is the definition commonly used in ship hydrostatics. A change of the trim angle θ does not influence the heel angle ϕ. The two angles are the *Euler angles* associated with Oy-axis. The third angle associated with the rotation of Oy-axis projection onto the horizontal plane (i.e. yaw) is not present as the rotation plane is fixed in space. Under the above given assumption b) any yaw-inducing moments are not considered in ship hydrostatics.
- ⇨ The righting arm GZ is the arm of the couple of forces forming the righting moment, i.e. the distance, measured in the rotation plane, between the action line of gravity force and that of buoyancy force.
- ⇨ As the righting moment is all the time parallel to the trace of water on PS, the righting moment work is the integral of the moment, respective to the heel angle ϕ. Simultaneously this is the least work which is to be performed in order to heel the ship up to a given angle ϕ . In other words, for a ship of a fixed trim or that not fully balanced the work of righting moment is greater.

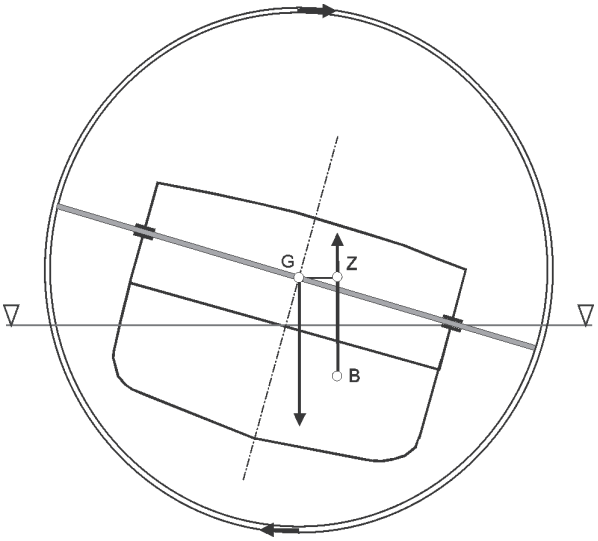

Fig. 2. *Rotation plane of free-floating ship which trims in PS*

It can be observed that the projection of Oy-axis onto the horizontal plane is perpendicular to the trace of water on PS. Hence the presented model of the heeling moment action strictly corresponds to the heeling moment due to a shift of cargo in ship's transverse plane. This deals also with the heeling moment of ro-ro ships in the damage condition, resulting from the accummulation of water on the car deck when a symmetrical midship compartment has been flooded. For the same reason the curve of righting arms measured by means of the Di Belli method[3] is strictly consistent with the above given model of inclinations. Finally, the heeling moment of fixed direction in space, parallel to the trace of water on PS, is an accepted idealization of the wind-induced moment.

BASIC RELATIONSHIPS

A right hand side coordinate frame Oxyz, shown in Fig.3, fixed to the ship, is assumed. The point O is identical with the point K, Oy-axis points port, and Oz-axis – upwards.

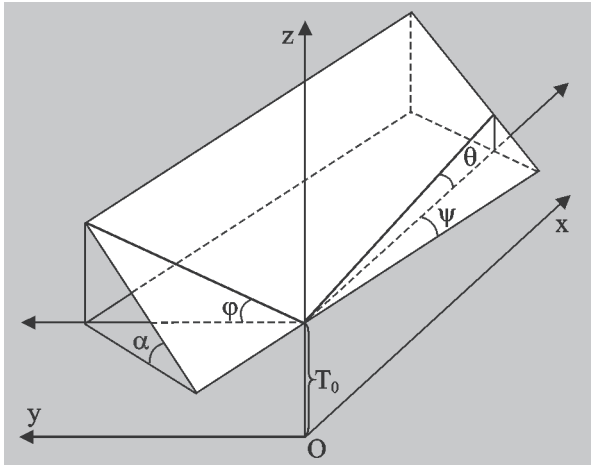

Fig. 3. *The right hand side coordinate frame Oxyz*

An arbitrary attitude of the waterplane can be described by the equation :

$$z = T_0 + x\,tg\theta + y\,tg\varphi \qquad (1)$$

in which three independent parameters appear. These are :

- ✦ the angle θ called the trim angle which is the slope angle of the trace of water on PS relative to Ox- axis

- the angle φ which is the slope angle of the trace of water on the midship plane relative to Oy-axis, and
- T_o – draught of Oz-axis.

The above mentioned angles are positive when a positive increment of *z* corresponds to a positive increment of *x* (or *y*) , as shown in Fig.3. Therefore the trim angle $\theta > 0$ is positive when the ship is trimmed by bow, and the angle $\varphi > 0$ is positive when it is heeled a-port. Both the angles are easy to be measured as :

$$tg\theta = \Delta T_{DR}/L_{pp} \text{ and } tg\varphi = \Delta T_{LP}/B$$

where :

ΔT_{DR} – difference of bow and stern draughts measured at the respective perpendiculars

ΔT_{LP} – difference of port and starboard draughts measured midships.

The angles φ and θ unambiguously describe position of the ship against water-level (or water-level against the ship) and are called the *analytical angles*. From the analytic geometry it results that the vector **R** normal to the waterplane given by (4) has the components :

$$\mathbf{R} = (tg\theta\ ,\ tg\varphi\ ,\ -1) \tag{2}$$

which points downwards and its absolute value equals :

$$R = \sqrt{1 + tg^2\theta + tg^2\varphi} \tag{3}$$

Hence the versor **n** normal to the waterplane and pointing upwards is equal to :

$$\mathbf{n} = -\mathbf{R}/R \tag{4}$$

The angle α contained between the water-level and the base plane BP (or initial waterplane) is one of the heel angles taken for calculation of the curve of righting arms. The angle between the planes is the same as that between the versors **n** and **k** normal to them. As a result, $\cos\alpha = \mathbf{k} \cdot \mathbf{n}$. Therefore :

$$\cos\alpha = 1/R = 1/\sqrt{1 + tg^2\theta + tg^2\varphi}$$

Hence :

$$tg\alpha\sqrt{tg^2\theta + tg^2\varphi} \tag{5}$$

The sign of the angle α is the same as that of the angle φ. Taking into account that $1/R = \cos\alpha$ the formula (4) yields the following components of the versor **n** :

$$\mathbf{n} = (-tg\theta\cos\alpha\ ,\ -tg\varphi\cos\alpha\ ,\ \cos\alpha) \tag{6}$$

The heel angle ϕ is equal to the inclination angle of PS from the vertical. The angle is the same as that of Oy-axis relative to water-level. Hence $\cos(90° + \phi) = \mathbf{j} \cdot \mathbf{n} = n_y$. And, $\sin\phi = tg\varphi\cos\alpha$, or simpler :

$$tg\phi = \cos\theta tg\varphi \tag{7}$$

The rotation plane rotates around the rotation axis parallel to the direction of the heeling moment action, defined by the versor **e**. The rotation angle is equal to the angle ϕ . The heeling moment direction is parallel to the water-level trace line on PS, whose versor $\mathbf{e}_1 = (\cos\theta, 0, \sin\theta)$, see Fig.3. Hence $\mathbf{e} = \mathbf{e}_1$.

Righting arm

In the course of heeling the ship its displacement remains constant and its buoyancy centre shifts in the rotation plane perpendicular to the rotation axis. Therefore the following is yielded :

$$\mathbf{e} \cdot \mathbf{r} = 0 \tag{8}$$

for any heel angle ϕ, where :

$\mathbf{r} = (x_B - x_G\ ,\ y_B - y_G\ ,\ z_B - z_G)$ – buoyancy centre radius vector relative to the ship gravity centre $\mathbf{r} = \mathbf{GB}$.

The righting moment is given by the formula :

$$\mathbf{M} = \mathbf{r} \cdot \mathbf{n}\Delta \tag{9}$$

where :

$\Delta = \rho g \nabla$ - ship buoyancy.

The vector is parallel to the rotation axis **e**, hence :

$$M = \mathbf{e} \cdot (\mathbf{r} \cdot \mathbf{n})\Delta \tag{10}$$

Therefore the righting arm $GZ = M/\Delta$ is given by the formula :

$$GZ = \mathbf{e} \cdot (\mathbf{r} \cdot \mathbf{n})$$

which is a function of the heel angle ϕ defined by (7). It is worth mentioning that the angle $\phi \le \alpha$, which can be observed directly from the formula $\cos\alpha = \cos\theta\cos\phi$ obtained by dividing $\sin\phi$ by $tg\phi$. From (7) it also results that $\phi \le \varphi$. Therefore the actual rotation angle ϕ is never greater either than the angle α or the angle φ, which have been taken as the heel angles of free-floating ship, so far.

Metacentric radii

The buoyancy centre of the free-floating ship moves along a curve in the rotation plane which rotates as a disc around the rotation axis motionless in space. As the action lines of the buoyancy force are always vertical they are perpendicular to the actual waterplane. When changing the ship heel by dϕ the buoyancy force lines rotate also by the angle dϕ in the rotation plane, and their respective waterplanes – by the angle $d\alpha_1$ around the instantaneous axis of waterplane rotation, called the ship **floatation axis f**. The relationship between the differentials is given by the following formula, [4] :

$$d\alpha_1\cos\chi = d\phi \tag{11}$$

where :

χ – the angle defining situation of the floatation axis relative to the rotation axis $\mathbf{e} = \mathbf{e_1}$, being the PS trace line on waterplane.

The equation (11) reflects the fact that small angles have vectorial features. Hence the angle dϕ is nothing else but the projection of the waterplane rotation angle $d\alpha_1$ onto the rotation axis **e**. In general case the angle $d\alpha_1$ is not equal to the change of the slope angle dα of waterplane relative to BP; the equality occurs only when the floatation axis **f** is parallel to the intersection edge of BP and water-level (see Fig.3).

The metacentric radius is understood as the curvature radius of the curve of buoyancy centres in the rotation plane; it depends on the angle ϕ. Translation of the buoyancy centre along the arc of the curve of buoyancy centres amounts to $ds = r_f d\alpha_1 = BMd\phi$. On accounting for the formula (11), the metacentric radius can be determined by the formula :

$$BM = \frac{r_f}{\cos\chi} \tag{12}$$

where :

$$r_f = (1/\nabla)\sqrt{I_f^2 + D_f^2}$$

f – instantaneous ship's floatation axis passing through the floatation centre F (the waterplane centre of gravity)

∇ – ship's hull volumetric displacement

I_f and D_f – transverse and deviation (cross-product) inertia moment of the instantaneous waterplane, respectively, associated with the floatation axis and floatation centre F.

The quantity r_f is a proportional coefficient between the buoyancy centre translation ds and the angle $d\alpha_1$.

The centre of buoyancy translates in the rotation plane, in parallel to the instantaneous waterplane (water-level). Therefore the buoyancy centre translation vector $d\mathbf{r} = (\mathbf{n} \cdot \mathbf{e})ds$.

Floatation axis

As it can be observed the metacentric radius of the free--floating ship , at a given heel angle, depends on location and orientation of the instantaneous floatation axis **f**. If the waterplane is rotated by the angle $d\alpha_1$ the transverse component of the buoyancy centre translation, BC, relative to the floatation axis (Fig. 4) is proportional to I_f, and the longitudinal component of this translation, AB,– to D_f, which results from the Euler's theorem of equi-volume waterplanes; this is the reason that the expression for the resultant translation AC, equal to $ds = r_f d\alpha_1$, appears in (12).

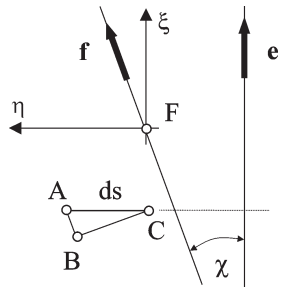

Fig. 4. *Waterplane top view*

It is required the resultant translation to be normal to the direction of heeling moment action (the rotation axis **e**). In order to obtain this the angle C in Fig.4 must be equal to χ, which results from the properties of the angles having correspondingly perpendicular arms. Therefore the floatation axis slope angle relative to the rotation axis has to satisfy the following equation :

$$\mathrm{tg}\chi = D_f / I_f \tag{13}$$

The angle χ has the same sign as that of the waterplane deviation moment (in Fig.4 - positive). It should be remembered that the moments D_f and I_f also depend on χ. By applying the relationships resulting from the Mohr circle [4,12], known from the theory of strength of materials, they can be represented as follows: $D_f = D'$, and $I_f = I + a'$. The equation (13) obtains then the form : $D' - (I + a')\mathrm{tg}\chi = 0$, where the mark „ ' " stands for the quantities associated with the rotated coordinate system (ξ', η') whose axis ξ' coincides with the floatation axis **f**, and its origin is located in the floatation centre F; (the system is not shown in Fig. 4). The quantities marked „ ' " are expressed by means of the quantities taken from the system (ξ, η) :

$$D' = D\cos 2\chi + a\sin 2\chi \equiv r\sin(2\gamma + 2\chi)$$

$$a' = a\cos 2\chi - D\sin 2\chi \equiv r\cos(2\gamma + 2\chi)$$

where : $a = \frac{1}{2}(I_{\xi\xi} - I_{\eta\eta})$ $I = \frac{1}{2}(I_{\xi\xi} + I_{\eta\eta})$ and

$D = I_{\xi\eta}$, $I_{\xi\xi}$, $I_{\eta\eta}$ - waterplane deviation moment, transverse and longitudinal inertia moment, respectively, in the system $\xi\eta$ (Fig.4) whose origin coincides with the floatation centre F, and the axis ξ is parallel to the rotation axis $\mathbf{e} = \mathbf{e}_1$ (a trace of PS on the waterplane).

The quantities D' and a' determine the parametric equation of the Mohr circle shown in Fig.5. When applying the introduced notation the equation (13) gets the following form :

$$r\sin(2\gamma + 2\chi) - [I + r\cos(2\gamma + 2\chi)]\mathrm{tg}\chi = 0 \tag{14}$$

where :

$$r = \sqrt{a^2 + D^2}\ , \quad 2\gamma_o = \mathrm{arctg}(D/a)$$

$2\gamma = 2\gamma_o$ if $a > 0$, in the opposite case : $2\gamma = 2\gamma_o + 180°$

The equation (13) having the quantities marked „ ' " is easier to be solved, and the equation (14) more simple for the geometrical interpretation shown in Fig.5; where *a* and γ_o are assumed negative.

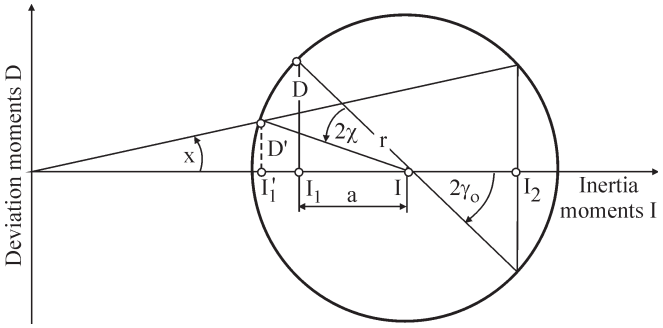

Fig. 5. *Mohr circle and geometric characteristics of waterplane*

When $\cos 2\chi$ and $\sin 2\chi$ appearing in (13) is expressed by $\mathrm{tg}\chi$ the equation (13) can be reduced to the simple 1st order equation :

$$D = (I - a)\mathrm{tg}\chi \tag{15}$$

Therefore : $\mathrm{tg}\chi = D/I_{\eta\eta}$

where : $|\chi| \le \arcsin(r/I)$ – see Fig.5.

As the angle χ is known, the quantities $D_f = D'$ and $I_f = I + a'$, necessary to express the radius on the basis of (12), as well as direction of the floatation axis, are defined. The floatation axis versor is given by the formula :

$$\mathbf{f} = \mathbf{e}\cos\chi + (\mathbf{n} \cdot \mathbf{e})\sin\chi \tag{16}$$

The equation (13) results from the asssumption that : $\mathbf{e} \cdot d\mathbf{r} = 0$, i.e. that the buoyancy centre translation in the ship-fixed coordinate system is normal to the rotation axis. It would be this way if the rotation axis were fixed to ship; however the axis is fixed in space but this does not mean it is fixed to the ship. It can be observed that when changing the heel also, in general, the trim has to be changed to balance the ship, which results in changing the orientation of the axis $\mathbf{e}_1 = (\cos\theta\ ,\ 0\ ,\ \sin\theta)$ relative to ship, determined by a trace of water on PS.

After differentiation of the equation (8) the following is obtained : $\mathbf{e} \cdot d\mathbf{r} = -d\mathbf{e} \cdot \mathbf{r}$, i.e. that the buoyancy centre translation in the hull-fixed coordinate frame is not strictly normal to the rotation axis. It should be intuitively obvious : the buoyancy centre translation in the ship-fixed frame has to be oblique to it as the buoyancy centre is to be permanently located in the rotation plane which changes its orientation relative to ship during inclinations. When this is accounted for, the following relationship for the angle χ between the floatation axis and rotation axis is obtained [4] :

$$\mathrm{tg}\chi = \frac{D}{I_{\eta\eta} - BZ\nabla} = \frac{D}{\nabla\left(BM_L - BZ\right)} \tag{17}$$

where :

BZ = $-\mathbf{r} \cdot \mathbf{n}$ – is the height of the gravity centre over the buoyancy centre (Fig.2)

BM_L – is the longitudinal metacentric radius represented by the bracketed term in (17).

As the term $BZ\nabla$ is negligibly small in comparison with the longitudinal inertia moment of waterplane, $I_{\eta\eta}$, the equation (17) practically yields the same solution as the equation (15).

Hence it can be observed that to determine the longitudinal radius of free-floating ship at a given heel angle it is necessary to know three geometrical characteristics of waterplane, viz. its deviation moment and transverse and longitudinal inertia moments in the $\xi\eta$ coordinate system associated with the rotation axis $\mathbf{e} = \mathbf{e}_1$ (a trace of PS on the waterplane) and the buoyancy centre. In calculating these characteristics it should be accounted for that the water trace lines on frame planes are not normal to the water trace line on PS. Denoting this angle by $90° + \beta$ the following is obtained : $\cos(90° + \phi) = \mathbf{e}_1 \cdot \mathbf{e}_2$, where : $\mathbf{e}_2 = (0 , \cos\varphi , \sin\varphi)$ is unit versor of the trace of water on frame planes (Fig.3).

Hence :

$$\sin\beta = -\sin\theta\sin\varphi \tag{18}$$

The way of calculation of the geometrical characteristics of the waterplane arbitrarily heeled relative to ship is discussed in [4] and [13].

When the floatation axis **f** is known it is easy to find the analytic angles φ and θ describing ship's location relative to water at a new heel angle. Namely, by changing the slope of the waterplanes relative to each other, by the angle $\Delta\alpha_1$, the rotation of the versor **n** around the floatation axis by the angle $\Delta\alpha_1$, is induced. Hence the new versor $\mathbf{n}_1$ is given by the formula :

$$\mathbf{n}_1 = \mathbf{n}\cos\Delta\alpha_1 + (\mathbf{f} \cdot \mathbf{n})\sin\Delta\alpha_1 \tag{19}$$

As the new versor **n** is known, the new analytical angles corresponding to the versor can be easily found by using the formula (6). Namely, $\mathrm{tg}\theta = -n_x/n_z$, and $\mathrm{tg}\varphi = -n_y/n_z$. Because the translation d**r** and the new waterplane slope angles are known, it is very fast to find a balanced location of buoyancy centre at the new heel angle enlarged by the angle $\Delta\phi$.

The versor **n** can be directly expressed by the angles θ and ϕ serving as degrees of freedom. To this end, in the formula (6) the expression $\cos\alpha = \cos\theta\cos\phi$ as well as that for $\mathrm{tg}\phi$ given by (7) should be accounted for. The following is immediately obtained :

$$\mathbf{n} = (-\sin\theta\cos\phi , -\sin\phi , \cos\theta\cos\phi) \tag{20}$$

Knowing the new versor **n**, one has as before : $\mathrm{tg}\theta = -n_x/n_z$, and $\sin\phi = -n_y$. It is not necessary to find $\mathrm{tg}\varphi = -n_y/n_z$, as in the first approximation the equation of new waterplane (in the ship-fixed frame) can be represented by the formula :

$$n_x(x - x_F) + n_y(y - y_F) + n_z(z - z_F) = 0 \tag{21}$$

where :

x_F, y_F, z_F - the coordinates of the previous floatation centre.

The equation (21) is more convenient than (1) , as $\mathrm{tg}\varphi$ and T_o tend to infinitely large values along with the heel angle increasing. The equation (1) is necessary to start calculations. The waterplane given by (21) is neither equi-volume nor balanced one. Correct values of draught and trim can be found by means of the method of successive approximations so as to maintain ship displacement constant and equal to an assumed value, and to make the equation (8) satisfied. The calculations become significantly shorter in case of making use of the properties of equi-volume waterplanes of free-floating ship. Within a finite interval of the heel angle $\Delta\phi$, such waterplanes roll on the surface of a cone whose parameters can be determined in advance [4]. The rolling waterplanes adhere to the cone along an instantaneous floatation axis.

Mechanism of equi-volume heels

An infinitesimal rotation of waterplane around the floatation axis **f** can be considered as resulting from two rotations : ship's rotation by the angle $d\phi$ around the rotation axis $\mathbf{e} = \mathbf{e}_1$ (trace of water on PS), and ship's rotation by the angle $d\theta$ around the normal to PS. The directed angle $\mathbf{j}d\theta$ is inclined by the angle ϕ relative to water-level. As small rotations have vectorial properties the directed angle $\mathbf{f}d\alpha_1$ is the resultant of two components : parallel and normal to the rotation axis **e** :

$$\mathbf{f}d\alpha_1 = (d\phi , -d\theta\cos\phi) \tag{22}$$

The components are defined in the $\xi\eta$ coordinate frame (see Fig.4). The normal component to the rotation axis, equal to $-d\theta\cos\phi$ is further denoted $d\alpha_2$. The directed angle $\mathbf{f}d\alpha_1$ is inclined by the angle χ to the rotation axis (ξ-axis). It can be seen in Fig.4 that the positive normal component $d\alpha_2$ corresponds to the positive angle χ, and the trim change is negative (by stern), therefore the normal component of the opposite sign must be applied. The projection of $d\alpha_1$ onto the rotation axis yields from the relationship (11). Taking into account the relationships inherent to rectangular triangles, one can determine the normal component $d\alpha_2$ in three different ways :

$$d\alpha_2 = d\alpha_1\sin\chi = d\phi\,\mathrm{tg}\chi = -d\theta\cos\phi \tag{23}$$

From this formula it results that :

- the more inclined the floatation axis from the rotation axis, the greater changes of ship trim during heeling, which is consistent with intuition
- when $\chi = 0$, i.e. $\mathbf{f} = \mathbf{e}$, ship trim does not change due to the waterplane rotation itself as in the case of fixed-trim ship
- for $\phi = 90°$ (PS is then horizontal), $\chi = 0$, i.e. the rotation axis (which does not then exist in the sense of trace of water on PS) determines the floatation axis **f**.

The rotation angle of PS around the normal , equal to $\mathbf{j}d\theta$, has also the vertical component : $-d\theta\sin\phi$. It makes the angle χ changing as a result of a change of orientation of the rotation axis (relative to ship hull), which occurs in the course of trimming. The change of the angle χ, which results from the change of orientation of the rotation axis only, is further denoted by $d\chi_o$. Hence the angle $d\chi_o = -d\theta\sin\phi$. Accounting for the equation (23), one obtains :

$$d\chi_0 = d\alpha_1\sin\chi\,\mathrm{tg}\phi = d\phi\,\mathrm{tg}\chi\,\mathrm{tg}\phi \tag{24}$$

If for a new waterplane the floatation angle χ changes by $d\chi$ the new floatation axis rotates against the previous one by the angle $d\chi_f = d\chi - d\chi_o$, equal to the difference of both the changes. When the angle $d\chi_f > 0$ is positive then the new floatation axis **f** shifts towards the heel , i.e. it departs from the rotation axis.

The equi-volume waterplanes roll on a cone whose axis is inclined relative to them by the angle ε determined by the following formula :

$$\mathrm{tg}\varepsilon = d\chi_f/d\alpha_1$$

To find the formula is very simple : it is enough to observe that $\mathrm{tg}\varepsilon$ is the ratio of the radius and the generatrix of the cone. When the angle $d\chi_f > 0$ is positive the cone is located above the waterplanes, otherwise – below them. The vertex of the cone is located in the distance *l*, of the generatrix from the floatation centre F, given by $l = -d\eta'_F/d\chi_f$, where $d\eta'_F$ is the translation of the floatation centre perpendicular to the floatation axis (when $l > 0$, the vertex is located fore). Taking into account that $d\eta'_F = r_F d\alpha_1$ one obtains :

$$l = -r_F d\alpha_1/d\chi_f = -r_F/\mathrm{tg}\varepsilon$$

where :

$r_F = dI_f/dV$ – differential metacentric radius (curvature radius of the curve of floatation centres).

From the formula it results that the cone base radius at the level of the floatation centre equals the differential metacentric radius.

The normal waterplane rotation component $d\alpha_2$ represents the ship trim angle measured in the vertical plane passing through the trace of water on PS. If ship heel is enlarged by $d\phi$, the buoyancy centre translation perpendicular to the rotation angle is proportional to $Dd\phi$, where : D - waterplane deviation moment in the $\xi\eta$ coordinate frame (Fig.4) .

The translation must be compensated by the trim $I_{\eta\eta}d\alpha_2$. Equating them to each other one gets $d\alpha_2 = (D/I_{\eta\eta})d\phi$. Accounting for that $tg\chi = d\alpha_2/d\phi$, one obtains the formula (15). A more exact solution can be obtained by using the metacentric formula for $d\alpha_2 = (D/\nabla GM_L)d\phi$, where : $GM_L = BM_L - BZ$ is the longitudinal metacentric height. As $tg\chi = d\alpha_2/d\phi$, the above gives the formula (17) provided before without derivation. The formula accounts for the rotation plane slope change defined in the hull-fixed coordinate frame, which results from the ship trim change.

(***to be continued***)

NOMENCLATURE

a	-	height of gravity centre over buoyancy centre in upright position of ship
B	-	buoyancy centre
BM	-	transverse metacentric radius
BM_L	-	longitudinal metacentric radius
BP	-	baseplane
BZ	-	height of gravity centre over buoyancy centre
e	-	direction of rotation axis (versor normal to rotation plane)
$\mathbf{e}_1$, $\mathbf{e}_2$	-	versors of trace of water on PS and on midship plane, respectively
f	-	versor of floatation axis
F	-	freeboard
g	-	gravity acceleration
G	-	ship gravity centre
GM	-	metacentric height
GZ	-	righting arm
i, **j**, **k**	-	versors of the ship–fixed coordinate frame whose origin is in the point K (intersection point of the plane of symmetry, PS, midship plane and base plane BP)
l, l_d,	-	righting arm and dynamic arm, respectively
L, B, T	-	length, breadth and mean draught of ship, respectively
n,	-	upward pointing versor nomal to waterplane
PS	-	ship plane of symmetry
SOLAS	-	Safety of Life at Sea
SWATH	-	Small Waterplane Hull
T_o	-	draught of z-axis
WEGEMT	-	European Association of Universities in Marine Technology
∇	-	volumetric displacement of ship
α	-	angle between initial waterplane and water-level
β	-	angle between water trace lines on PS and midship plane
Δ	-	ship buoyancy (weight of the displaced water)
Δl	-	correction of righting arm obtained by means of cross-curves of stability, accounting for oblique translation of gravity centre relative to rotation plane at changing the height of ship gravity centre over BP
η	-	rotation angle of plane of rotation
θ	-	slope angle of trace of water on PS relative to x-axis of ship
ρ	-	water density
φ	-	slope angle of trace of water on the stations relative to y-axis of ship
ϕ	-	angle of PS inclination from the vertical
ϕ_V	-	angle of vanishing stability
χ	-	angle between floatation axis and rotation axis
ψ	-	angle between water-level trace line and PS trace line on initial waterplane

[1] „Fix in space" does not mean : fixed relative to the ship hull coordinate system.

[2] In case of the objects arbitrarily situated relative to the heeling moment vector or wind direction (e.g. semi-submersible floating units) the comments concerning PS should be applied to the reference plane initially situated perpendicularly to the wind direction and rotating together with the object in question. For the ship unsymmetricaly flooded this is the plane parallel to the main inertia axis of the waterplane in ship's upright position.

[3] In the Di Belli method, a heel angle of ship model, induced by shifting a weight along an arm perpendicular to PS, is measured. The heel angle is the inclination angle of the arm against water-level.

BIBLIOGRAPHY

1. Wimalsiri, W. K.: *Design of ro-ro cargo ships with particular reference to damage survivability*. PhD thesis. Dept. of Marine Technology, University of Newcastle upon Tyne. 1991
2. Pawłowski, M.: *On the roll angle for a freely floating rig*. Proceedings of 9th Int. Symposium on Ship Hydromechanics HYDRONAV'91, Gdańsk–Sarnówek. September 1991, Vol. I also in: Budownictwo Okrętowe i Gospodarka Morska, November 1991
3. Pawłowski, M.: *Some inadequacies in the stability rules for floating platforms*. Naval Architect, No. 2, 1992
4. Pawłowski, M.: *Advanced stability calculations for a freely floating rig*. Proceedings of 5th Int. Symposium on Practical Design of Ships and Mobile Units PRADS'92. Newcastle upon Tyne. 1992, Vol. II also in: Report, Dept. of Marine Technology, University of Newcastle upon Tyne. November 1991
5. Kaźmierczak, J.: *Ship floatability and stability* (in Polish). Wydawnictwa Komunikacyjne (Transport Publishing House). Warszawa, 1954
6. Staliński, J.: *Ship theory* (in Polish). Wydawnictwo Morskie (Maritime Publishing House). Gdynia, 1961
7. Rahola, J.: *The judging of the stability of ships and the determination of the minimum amount of stability*. PhD thesis. University of Helsinki. 1939
8. International Maritime Organisation (IMO) : *Recommendation on intact stability criteria for passenger and cargo ships under 100 metres in length*. Resolution A.167 (ES.IV). London, 1987
9. International Maritime Organisation : *Subdivision and damage stability of cargo ships, chapter II–1, part B–1, SOLAS Convention*. Consolidated Edition. 1997
10. Pawłowski, M.: *A closed form assessment of the capsizal probability – the s_i factor*. Proceedings of WEGEMT Workshop on Stability of Ships. Technical University of Denmark (DTU). Lyngby. October 1995
11. Vassalos, D., Pawłowski, M., and Turan, O.: *Criteria for survival in damaged condition*. Proceedings of Int. Seminar on the Safety of ro-ro Passenger Vessels. RINA (Royal Institution of Naval Architects). London. June 1996 also in: *Dynamic stability assessment of damaged passenger ro-ro ships and proposal of rational survival criteria*. Marine Technology, Vol. 34, No. 4, October 1997
12. Huber, M. T.: *Technical stereomechanics (strength of materials)* (in Polish). Ed. II. PWN (State Scientific Publishing House). Warszawa, 1958 also e.g .: Parry, R. H. G.: *Mohr circles, stress paths and geotechnics*. E & FN Spon. London, 1995
13. Siemionov-Tian-Shansky: *Statics and dynamics of ships*. Peace Publishers. Moscow, 1963, also in Russian: *Statika i dinamika korabla*. Sudostrojenie. Leningrad, 1973

CONTACT WITH THE AUTHOR

Maciej Pawłowski, Assoc.Prof.,D.Sc.
Faculty of Ocean Engineering
and Ship Technology,
Gdańsk University of Technology
Narutowicza 11/12
80-952 Gdańsk, POLAND
e-mail : mpawlow@pg.gda.pl

Statistical investigations of fast changeable processes occurring in ship piston combustion engine

Zdzisław Chłopek
Warsaw University of Technology
Leszek Piaseczny
Polish Naval University

ABSTRACT

Combustion piston engine is one of the devices in which fast changeable processes occur in operational conditions. In this paper are presented basic problems associated with research on fast changeable processes occurring in diesel engines , exemplified by the processes of indicated pressure and fuel pressure injected to engine's cylinder. Dynamical characteristics of the investigated processes were analyzed and problems of synchronous averaging of pseudo-periodical signals were considered in order to limit high frequency noise content in useful signal. Some limitations of elimination effectiveness of high frequency noise from tested signals have been revealed.

Keywords : piston combustion engine, fast changeable processes, stochastic processes, high frequency noise

INTRODUCTION

Investigations of fast changeable processes, related to the dynamical features characteristics typical for operational conditions of devices, cause many methodological problems. This is especially important because of a high level of ignorance on disturbances of the processes associated with measurement systems as well as occurrence – in real objects – of factors not directly accounted for in testing program. The piston combustion engine is a typical object in description of which such problems appear [3 ÷ 6].

The processes occurring in the combustion engine can be classified from the point of view of their dynamical features, and a role they play in the engine's operation, namely [3] :

- processes associated with particular working cycles of the engine as well as the fast changeable ones in comparison with those characteristic for the typical use of the engine
- processes associated with the typical use of the engine
- processes associated with service (tribological) wear of the engine as well as slowly changeable ones in comparison with the processes characteristic for the typical use of the engine.

The first group of the processes contain all the processes connected with engine's cycle. Processes not fully connected with the cyclic work of the engine, however generated by it, e.g. vibration of its elements, can be also considered as belonging to that group. Frequencies of the processes, conventionally considered as characteristic[1)] for them, should be at least one-order higher than those of engine working cycles as they occur in intervals corresponding to fragments of single cycles [3].

The processes characteristic for the typical use of the engine are associated with operational forcing factors affecting the engine. The main service forcing factors are the following : control of the engine by its operator, and its loading from the side of power consumer.

The power consumer reacts by rate of its task realization, and the engine – by changing its rotational speed. On the basis of analyses of the processes it can be stated that the characteristic frequencies of the processes associated with the typical use of the engine are contained within the interval (0.01 ÷ 10) Hz, with a large safety margin [3].

The slowly changeable processes in comparison with those connected with the typical use of the engine are of entirely different dynamical character. To this category can be counted the thermal processes which characterize engine's thermal state described by the set of temperatures of engine parts and systems. Such processes have time constants in the order of several or a dozen or so minutes, a few dozen of seconds at least. The processes even more slowly changeable than the thermal ones are those describing atmospheric conditions , all the more tribological processes associated with engine's wearing [3].

In the combustion engine it is characteristic – due to its working principle – that the fast changeable processes, especially those connected with working cycles, are pseudo-periodical. The pseudo-periodicity, but not periodicity, of the processes results : firstly from the fact that periodic function is determined for unlimited set of independent variable values,

1) The conventional notion of „characteristic frequencies" is assumed equivalent to the range of frequency values for which amplitudes of frequency representation of a process have significant values arbitrarily assumed by a researcher (and sometimes customary assumed by specialists to be valid) [3].

and secondly from that the investigated processes are real. Due to the pseudo-periodicity of the processes associated with particular engine working cycles, high-frequency disturbances of signals can be modelled as the signal amplitude disturbances and also as independent variable ones. In this case the independent variable is usually :

time - t ; crank angle - α.

Let x(t) be a pseudo-periodical signal such that :

$$\left|x(t)-x(t+j\cdot T)\right|<\varepsilon \tag{1}$$

where :

particular phase j = 1, 2, ..., N
$\varepsilon > 0$
T - a quantity estimated as a tested signal pseudo-period.

Therefore the inaccuracy ε depends on :

- high-frequency noise amplitudes
- characteristics of the set of successive pseudo-periods, $\{T_i\}$, where : i = 1, 2, ..., N – 1.

The synchronous averaging of the signal x(t) consists in determining the function [1, 12, 13] :

$$\overline{x}(t)=\frac{1}{N}\sum_{j=0}^{N}x(t+j\cdot T) \tag{2}$$

On the assumption that values of elements of the set $\{T_i\}$ are constant, the synchronous averaging of the signal makes it possible – in compliance with the laws of large numbers (inequality of Chebyshev, laws of Markov and Chintsin [2, 9, 17]) – to significantly limit high-frequency noise content in useful signal, for a certain class of processes describing high-frequency noise, e.g. normal ones :

$$\lim_{N\to\infty}\left[\overline{x}(t)-x(t)\right]=0 \tag{3}$$

The most important limitations of effectiveness of the synchronous averaging of signals are the following problems : determination of a tested signal pseudo-period as well as of features of the set of particular pseudo-periods.

In the case of signal digital processing the accuracy of the pseudo-period estimation depends on [1, 3, 4, 12, 13] :

- resolution of quantization of the signal, that determines accuracy of assessing independent variable values
- sampling frequency which determines Nyquist frequency of an observed signal
- signal observation time deciding on frequency resolution of an observed signal.

Influence of sampling frequency on accuracy of pseudo-period estimation is solely theoretical because it is only required the sampling frequency to be at least two times greater than that corresponding to expected value of pseudo-period. In order to obtain a small inaccuracy value of pseudo-period estimator it is necessary to use a large value of quantization resolution as well as long observation times [1, 3, 4, 12, 13].

To satisfy the conditions is sometimes really difficult, e.g. when the conditions not directly accounted for in testing program influence qualification of processes as stationary ones – – in this case an increase of observation time can make it impossible to qualify a process as stationary one.

The other effectiveness limitation of the synchronous averaging of signals depends on how large deviations of particular pseudo-periods from a value estimated as representative for a tested signal, are. In the case of too large deviations the synchronous averaging of signal can lead to a significant limitation of amount of information about useful signal, hence – in fact – to generation of additional noise instead of limitation of noise content in a tested signal (it is obvious that any processing of signal inevitably contributes to noise generation [1, 3, 4, 12, 13]).

Effective improvement of quality of the synchronous averaging of pseudo-periodical signals occurring in piston combustion engine can be obtained by signal sampling in the domain of crankshaft rotation angle, but not in the domain of time [1, 3, 4, 12, 13]. This way influence of rotational speed fluctuations on effectiveness of the synchronous averaging of signals may be avoided.

INVESTIGATIONS OF THE PROCESSES OF INDICATED PRESSURE AND INJECTION PRESSURE

The presented basic problems associated with research on fast changeable processes occurring in diesel engines are here exemplified by the processes of indicated pressure and fuel injection pressure in cylinder. The investigations have been carried out at the laboratory stand equipped with 6AL 20/24 Sulzer ship diesel engine of 37.7 dm^3 piston displacement, 420 kW rated output and 750 min^{-1} rotational speed.

The tests were carried out in statical working conditions, i.e. those independent on time [3] in the frequency range corresponding to real engine working conditions. In Fig.1 the testing point of the engine in question is presented.

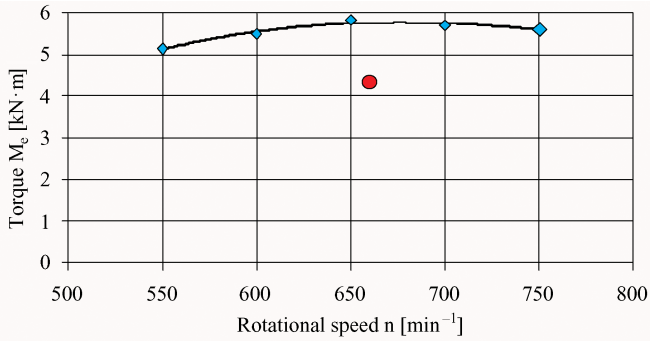

Fig. 1. *Testing point of the tested engine operating in compliance with rotational speed characteristics*

For testing the signals quantized by means of a 12–bit transducer and recorded at the sampling interval Δt = 50 μs , the sample sets of 32 000 elements each were used.

The analyses were performed in the domains of [1, 3, 12, 13, 17] :

- time
- process values
- frequency.

The recorded signals are presented in Fig.2 and 3.

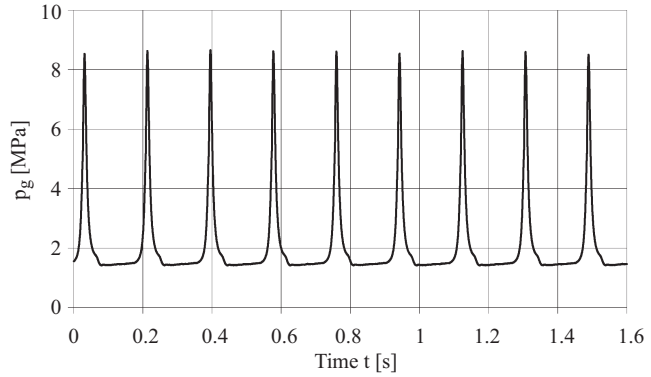

Fig. 2. *Indicated pressure* $\mathbf{p_g}$ *in function of time*

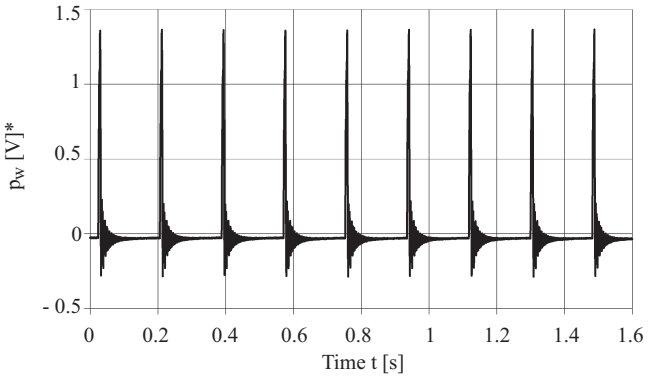

Fig. 3. Fuel injection pressure $\mathbf{p_w}$ *in function of time*

In Fig. 4 the correlation relationship of the indicated pressure and injection pressure is presented. The correlation coefficients are of relatively large values : beginning from 0.2441 of Kendall's τ and 0.2471 of Kendall's γ [2,9], 0.2855 of Spearman's range coefficient [2,9] up to 0.6079 of Pearson's linear coefficient [2, 9, 14], for this reason there is no ground to reject hypotheses on lack of correlation between analyzed signals (Fig.5).

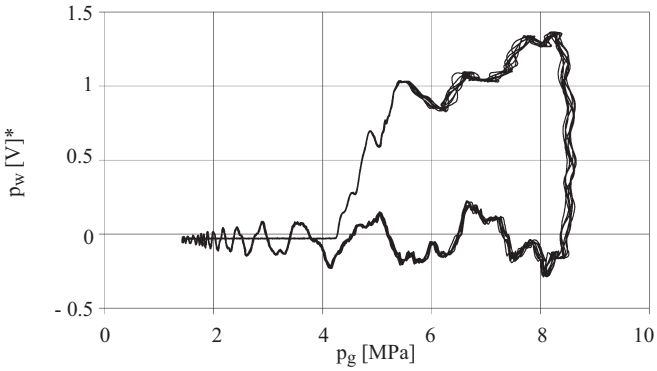

Fig. 4. Correlation relationship of injection pressure $\mathbf{p_w}$ *and indicated pressure* $\mathbf{p_g}$

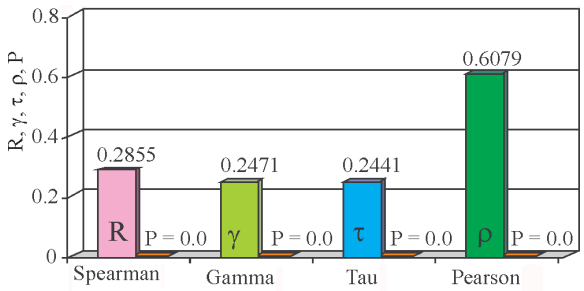

Fig. 5. The correlation coefficients of Spearman : **R** *, Kendall :* **γ** *and* **τ**, *and Pearson :* **ρ** *- for sets of indicated pressure and injection pressure, as well as the probability of non-rejection of hypotheses on lack of correlation of the sets ,* **P**

The tested signals were subjected to stationarity analysis [1, 12, 13, 17]. To this end the mean values and standard deviations were determined in particular phases corresponding to pseudo-periods (Fig.6 and 7). On the basis of the performed analysis the assumption on stationarity of the tested signals was adopted.

The signals of indicated and injection pressures were subjected to time and frequency analyses. For the investigations an algorithm based on Fourier's fast transformation as well as Hamming's five-sample-wide window was applied [1, 12, 13]. The signal power spectral density of indicated pressure and injection pressure, with eliminated linear trends, are presented in Fig.8.

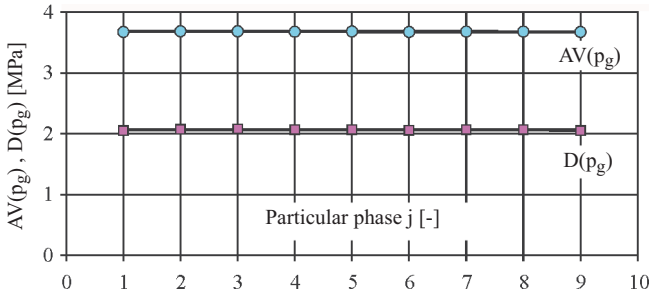

Fig. 6. Mean value **AV** *and standard deviation* **D** *of indicated pressure* $\mathbf{p_g}$ *in course particular phases*

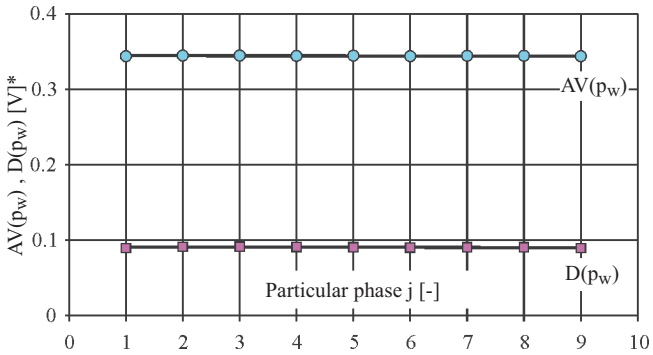

Fig. 7. Mean value **AV** *and standard deviation* **D** *of injection pressure* $\mathbf{p_w}$ *in course particular phases*

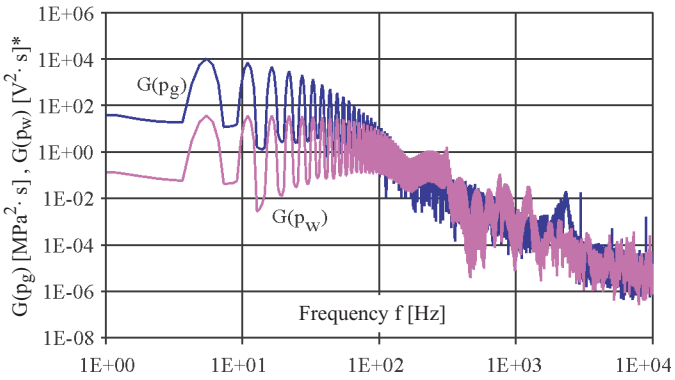

Fig. 8. Signal power spectral density **G** *of indicated pressure* $\mathbf{p_g}$ *and injection pressure* $\mathbf{p_w}$

The first maximum of power spectral density of both signals appears at the frequency f = 5.4931640625 Hz, which corresponds to the pseudo-period T = 1/f = 0.182044 s. The pseudo-period of that value corresponds to the rotational speed :

$$n = f \cdot 2 \cdot 60 \ [\text{min}^{-1}] \qquad (4)$$

where : frequency f [Hz]

On substitutions : n = 659.2 min^{-1} the mean rotational speed recorded during the test series at the frequency of 1 Hz, was equal to 659.3 min^{-1} [6]. On the basis of the results, inaccuracy of pseudo-period estimation of the tested signals can be assessed : it is smaller than 0.023%.

Also, the auto-correlation function of indicated and injection pressures was determined (Fig. 9).

Also, the results of the correlation analysis of signals confirmed the determined pseudo-period value : the maximum of correlation function occurred at the time-lag Δt = 0.182044 s. The mutual testing of the signals of indicated and injection pressures was also performed (Fig.10 and 11).

*) The injection pressure Pw was measured in voltage units and due to technical reasons it was not converted into pressure units

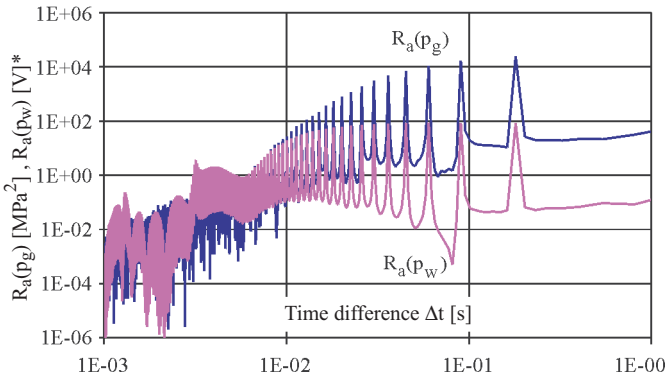

Fig. 9. *Auto-correlation function* $\mathbf{R_a}$ *of indicated pressure* $\mathbf{p_g}$ *and injection pressure* $\mathbf{p_w}$

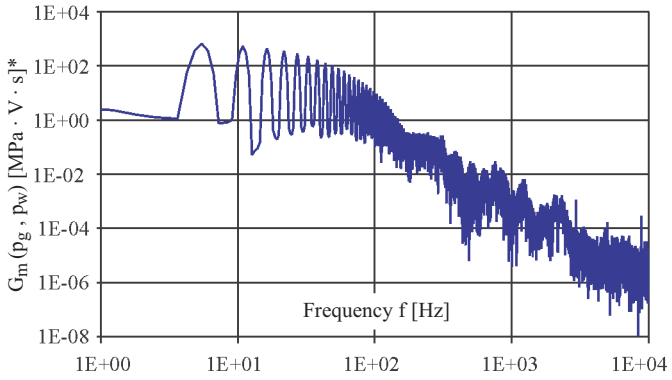

Fig. 10. *The module of mutual spectral density of power* $\mathbf{G_m}$ *of indicated* $\mathbf{p_g}$ *and injection* $\mathbf{p_w}$ *pressures*

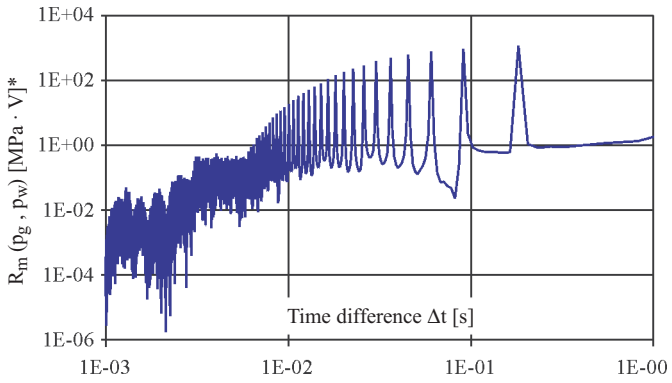

Fig. 11. *Mutual correlation function* $\mathbf{R_m}$ *of indicated* $\mathbf{p_g}$ *and injection* $\mathbf{p_w}$ *pressures*

This mutual testing of the signals confirmed the estimated pseudo-period value representative for the tested signals.

By making use of the determined pseudo-period value of the tested signals their synchronous averaging was performed. Before the synchronous averaging the courses were subjected to the lowpass filtering of 1 kHz limit frequency to decrease high-frequency noise content in the tested signals. For realization of the operation a filter with applied Fourier's fast transformation algorithm, was used [1, 4, 5, 12, 13].

In Fig.12 a fragment of the initial course and the averaged one of indicated pressure, and in Fig.13 – of injection pressure, was presented.

In both the cases the mean deviations of initial courses are rather small. The courses of the deviations in particular phases are presented in Fig.14 and 15, and the sets of all deviations – – in Fig.16 and 17.

Despite the relatively small deviations of signal values from the averaged one, the interference phenomenon is here characteristic, especially distinct for injection pressure the course of which shows content of high-frequency components of a greater amplitude than in the case of indicated pressure. The interferences occuring in the sets of deviations are due to : on one hand – real non-periodicity of the tested courses, on the other hand – very small difference of estimated pseudo-period and successive real pseudo-periods.

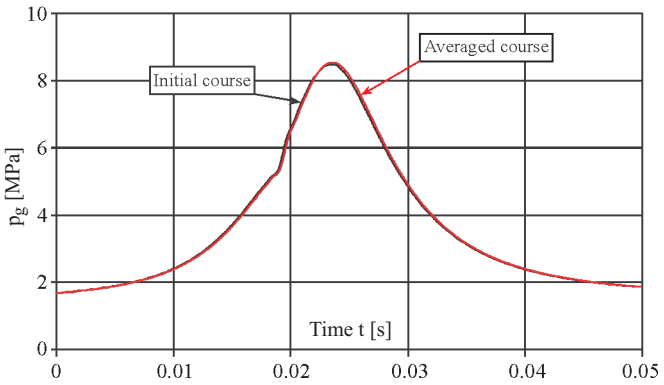

Fig. 12. *A fragment of the initial course and the averaged one of indicated pressure* $\mathbf{p_g}$

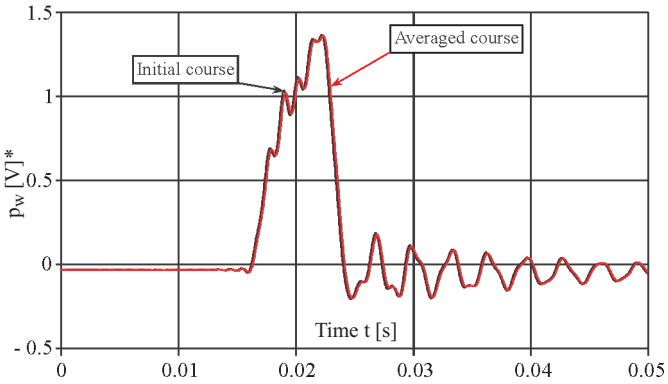

Fig.13. *A fragment of the initial course and the averaged one of injection pressure* $\mathbf{p_w}$

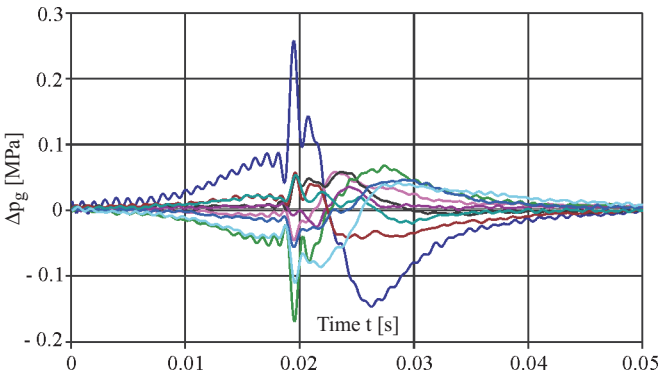

Fig. 14. *Fragments of the courses of deviations from the averaged value of indicated pressure* $\mathbf{\Delta p_g}$ *in particular phases*

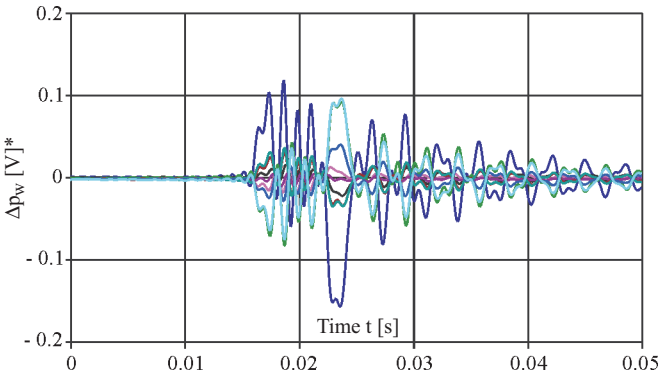

Fig. 15. *Fragments of the courses of deviations from the averaged value of injection pressure* $\mathbf{\Delta p_w}$ *in particular phases*

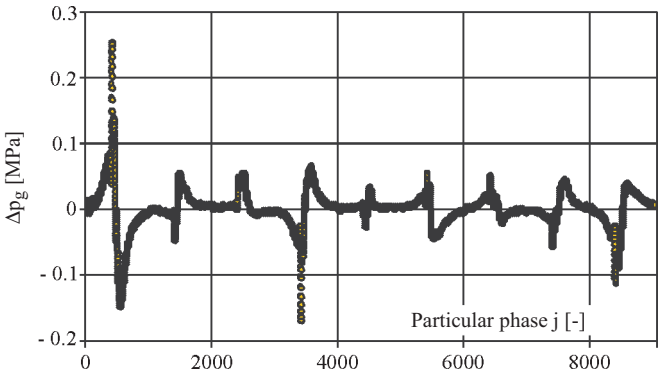

Fig. 16. Set of deviations from the averaged value of indicated pressure Δp_g *in particular phases*

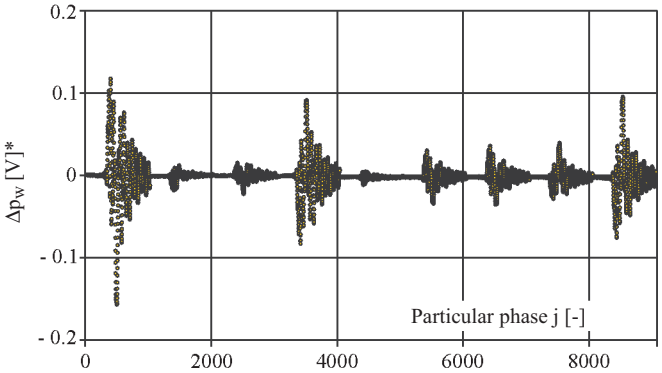

Fig. 17. Set of deviations from the averaged value of injection pressure Δp_w *in particular phases*

In Fig.18 and 19 are presented the results of analysis of standard deviation of the tested signals and deviations from their averaged value. Small values of standard deviations and deviations of these deviations, relative to the standard deviations of the initial signals, were observed : smaller – of about 1.5% - for indicated pressure, and greater – of about 5% - for injection pressure – in this case a greater content of high-frequency noise not eliminated from the initial signal, can be clearly observed (Fig. 20).

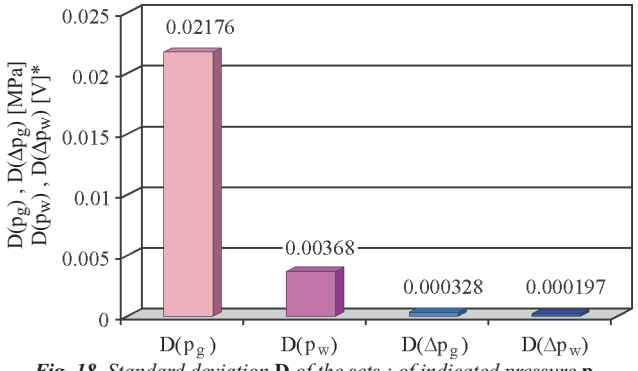

Fig. 18. Standard deviation **D** *of the sets : of indicated pressure* p_g *and of injection pressure* p_w *, as well as of deviations from averaged values of these pressures* Δp_g , Δp_w

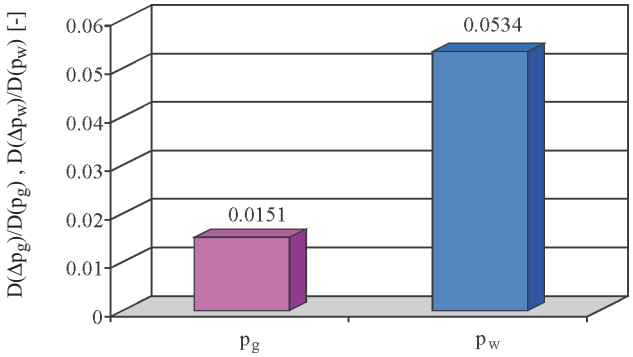

Fig. 19. Ratios of standard deviations **D** *of the sets: of deviations from averaged values of indicated and injection pressures,* (Δp_g , Δp_w) *as well as of indicated pressure* p_g *and injection pressure* p_w

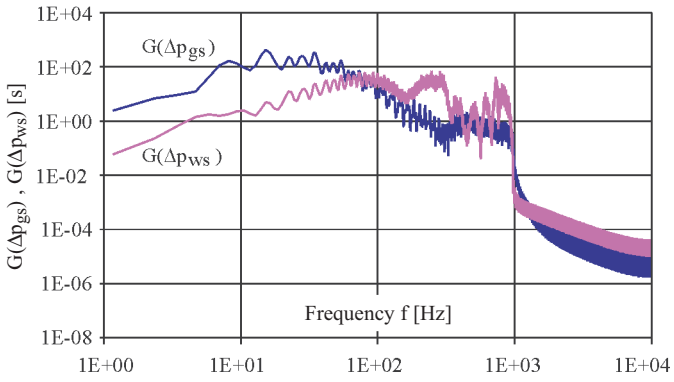

Fig. 20. Power spectral density **G** *of standardized deviations from averaged values of indicated and injection pressures* (Δp_{gs} , Δp_{ws})

Also, correlation relationship of deviations of the standardized indicated pressure (of the mean value equal to zero and standard deviation equal to 1 [1, 2, 9, 12, 13]) and deviations of the standardized injection pressure, was determined. The correlation coefficients of Spearman, Kendall and Pearson of the analyzed sets , as well as the probability of non-rejection of hypotheses on lack of correlation of the sets are presented in Fig.21 [2, 9, 14].

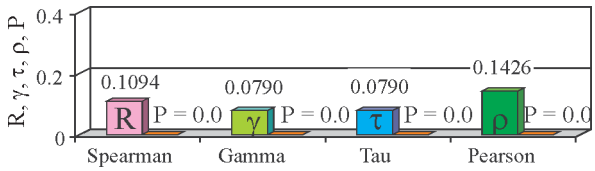

Fig. 21. Correlation coefficients of : Spearman, **R**, *Kendall,* γ *and* τ, *as well as of Pearson,* ρ, *of the sets of standardized deviations from averaged values of indicated pressure* Δp_{gs} *and injection pressure* Δp_{ws} , *and the probability of non-rejection of hypotheses on lack of correlation of the sets,* **P**

On the basis of the performed analysis it was stated that there is no ground to reject hypothesis on lack of correlation between the sets of standardized deviations from averaged values of indicated pressure and injection one.

The sets of deviations of the pressures in question as well as standardized deviations were analyzed in the value domain. In Fig.22 the histograms of standardized sets of deviations of indicated pressure and injection one from their averaged values, are presented, and in Fig.23 – the probability density of the tested sets.

Also, conformity of the tested sets to normal distribution was assessed. To this end the following hypotheses were applied: of Kolmogorov and Smirnov [2, 9, 10, 16], of Lilliefors [2, 9, 11], and of Shapiro and Wilk [2, 9, 15]. In Fig.24 for instance the Kolmogorov–Smirnov statistics of the sets of the standardized deviations of indicated pressure and injection pressure from their averaged values, are presented; the probability of non-rejection of the above mentioned hypotheses equals zero.

As a result of the tests of the analyzed sets it was stated that there has been no ground to accept the used hypotheses on conformity to normal distribution of the sets of standardized deviations of indicated and injection pressures from their averaged values. Probably, a big interference content in the analyzed sets to a large extent decided on the observed, different from normal, character of the analyzed deviations. In the case of strictly synchronous averaging the tested signals, the normally distributed deviations from averaged value should be rather expected.

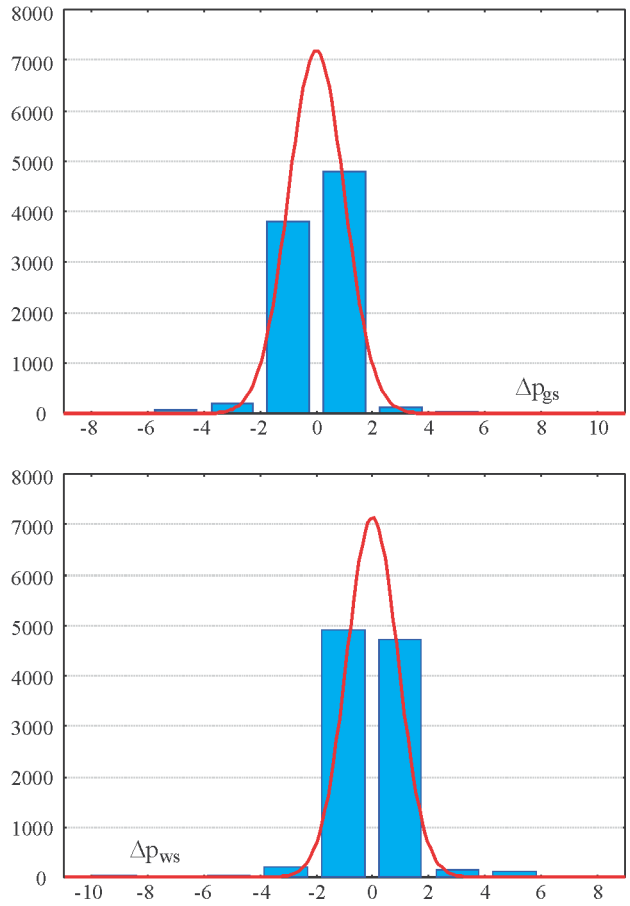

Fig. 22. The histograms of sets of the standardized deviations of indicated pressure , Δp_{gs} , and of injection pressure, Δp_{ws} , from their averaged values (continuous lines stand for respective normal distributions)

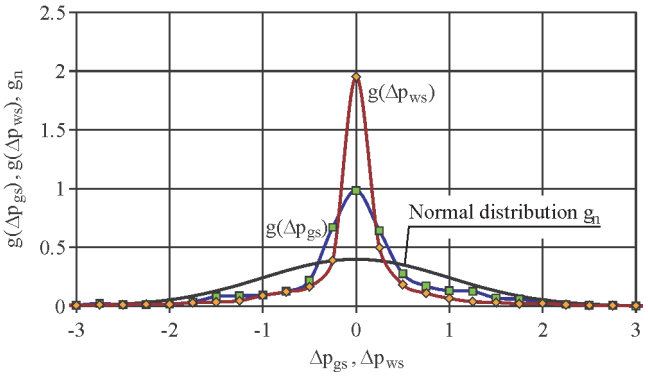

Fig. 23. The probability density **g** *of sets of the standardized deviations of indicated pressure, Δp_{gs} , and of injection pressure, Δp_{ws} , from their averaged values*

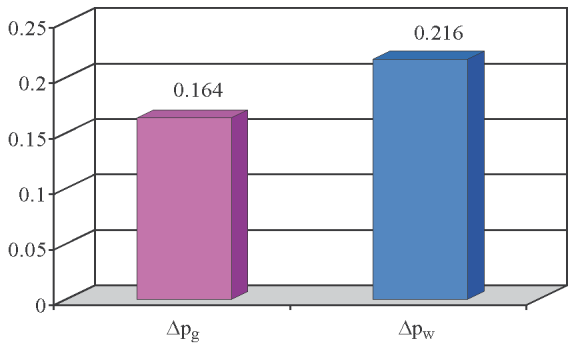

Rys. 24. The Kolmogorov–Smirnov statistics **d** *of the sets of the standardized deviations of indicated pressure Δp_g and injection pressure Δp_w from their averaged values*

SUMMARY

- Investigations of fast changeable processes make great difficulties which can result in over-interpretation of test results, namely in formulating judgements on investigated phenomena, on the basis of the investigation of features of measurement systems, as well as on the knowledge gained during analyzing the phenomena not directly accounted for in the test program. Therefore a formal critical analysis of measurement results, based on real knowledge on investigated phenomena as well as formal tools for processing the measurement results, is necessary.

- The example analyses presented in this paper have confirmed that it is reasonable to comprehensively test recorded signals as well as noise features. Such tests can a.o. to justify the thesis on a physical nature of noise eliminated from the initial signal. As a result of the analysis it can be also stated that the transformations performed on a recorded signal may be a factor deciding on the nature of noise. Such case was also revealed in this work: some features of the tested noise originated from the process of selecting it out of the initial signal, namely the interferences due to synchronous averaging.

- The comprehensive testing of recorded signals is necessary to avoid subject-matter errors difficult to be predicted in further analyses. Examples of such errors resulting from transformations of the signals containing noise of an unknown nature are numerous in the field of combustion engines; for instance, the determination of heat rate generated in engine cylinder, performed on the basis of indicated pressure signal. In this case noise due to numerical differentiation of indicated pressure is usually subjected to such procedures [4, 5].

NOMENCLATURE

AV – mean value
d – Kolmogorov–Smirnov statistics
D – standard deviation
f – frequency
g – probability density
G – spectral density of power
G_m – mutual spectral density of power
H – occurence frequency of a process value on histogram
M_e – effective torque
n – rotational speed
p_g – indicated pressure
p_w – injection pressure
P – probability of non-rejection of a hypothesis
R – Spearman's range correlation coefficient
R_a – auto-correlation function
R_m – mutual correlation function
t – time
T – signal pseudo-period
x – process
$\overline{x}$ – synchonously averaged process
Δt – time-lag

Δp_g – indicated pressure deviation
Δp_{gs} – standardized deviation of indicated pressure from its averaged value
Δp_w – injection pressure deviation
Δp_{ws} – standardized deviation of injection pressure from its averaged value

γ – Kendall's gamma correlation coefficient
ρ – Pearson's linear correlation coefficient
τ – Kendall's tau correlation coefficient

BIBLIOGRAPHY

1. Bendat J.S., Piersol A.G.: *Methods of analyzing and measuring the random signals* (in Polish). PWN (State Scientific Publishing House). Warszawa, 1976
2. Box G.E.P., Hunter W.G., Hunter J.S.: *Statistics for experimenters: An introduction to design, data analysis, and model building.* John Wiley & Sons. New York, 1978
3. Chłopek Z.: *Modelling of exhaust gas emission processes in service conditions of diesel engines* (in Polish). Prace Naukowe. Seria „Mechanika", (Scientific Bulletin, Mechanics series), issue 173. Publishing House of Warsaw University of Technology. Warszawa, 1999
4. Chłopek Z.: *On selected methods of numerical differentiation on the example of cylindrical pressure course differentiation*. Journal of KONES (Internal Combustion Engines). Gdańsk, 2001
5. Chłopek Z.: *The subject of task explicitness in numerical differentiation.* Journal of KONES (Internal Combustion Engines). Gdańsk, 2001
6. Chłopek Z., Piaseczny L.: *Research on statistical features of diesel engine in statical conditions of operation* (in Polish). Scientific Bulletin of Polish Naval University (to be published).
7. Chłopek Z., Piaseczny L.: *On role of modelling in scientific research* (in Polish). Zeszyty Naukowe Akademii Marynarki Wojennej (Scientific Bulletin of Polish Naval University). Vol. XLII, No.146. Gdynia, 2001
8. Chłopek Z., Piaseczny L.: *Remarks about the modelling in science researches.* Operation and Reliability, No. 4/2001
9. Fisz M.: *Calculus of probability and mathematical statistics* (in Polish). PWN (State Scientific Publishing House). Warszawa, 1967
10. Kolmogorov A.: *Confidence limits for an unknown distribution function.* Annals of Mathematical Statistics, No.12/1941
11. Lilliefors H. W.: *On the Kolmogorov–Smirnov test for normality with mean and variance unknown.* Journal of the American Statistical Association, No.64/1967
12. Oppenheim A.V., Schafer R.W.: Digital processing of *signals* (in Polish). WKŁ (The Publishing House for Traffic Services and Telecommunication). Warszawa, 1979
13. Otnes R.K., Enochson L.: *Numerical analysis of time series* (in Polish). WNT (Scientific-Technical Publishing House). Warszawa, 1978
14. *Pearson K.: On the theory of contingency and its relation to association and normal correlation*. Drapers' Company Research Memoirs. Biometric Ser. I., 1904
15. Shapiro S. S., Wilk M. B., Chen H. J.: *A comparative study of various tests of normality*. Journal of the American Statistical Association, No.63/1968
16. Smirnov N. V.: *Table for estimating the goodness of fit of empirical distributions*. Annals of Mathematical Statistics, No.19/1948
17. Sobczyk K.: *Methods of statistical dynamics* (in Polish). PWN (State Scientific Publishing House). Warszawa, 1973

CONTACT WITH THE AUTHOR

Zdzisław Chłopek, Assoc.Prof.
Automobiles and Building Machines Faculty,
Warsaw University of Technology
Narbutta 84
02-524 Warszawa, POLAND
e-mail : zchlopek@simr.pw.edu.pl

— — — — — — —

Prof. Leszek Piaseczny
Mechanic-Electric Faculty,
Polish Naval University
Śmidowicza 69
81-103 Gdynia, POLAND
e-mail : lpias@amw.gdynia.pl

Conference

COMPOWER'04

On 2-3 December 2004 Gdańsk University of Technology and Alstom Power Ltd organized the 3rd International Scientific Symposium on :

Technical, Economic and Environmental Aspects of Combined Cycle Power Plants

It was first of all aimed at drawing attention of engineers and economists onto application of turbines to propulsion and heating systems, especially those based on so called gas-steam cycles. They are characterized by technical, economical and ecological advantages such as :

- the improvement of the power plant performance
- the increase of the energy conversion efficiency
- the decrease of the coal consumption
- the decrease of the environmental pollution.

29 papers, split into 5 topical chapters, were prepared for presentation during the Symposium :

- *Modelling and simulation of turboset characteristics* (6 papers)
- *Neural network application to turboset simulation* (6 papers)
- *Turbine plant diagnostics* (4 papers)
- *Analysis and improvement of turbine plant characteristics* (8 papers)
- *Turbine plant operation, reliability and control* (5 papers).

The papers were mainly prepared by Polish scientific workers from : Institute of Fluid-Flow Machinery of Polish Academy of Sciences, Gdańsk University of Technology, Silesian University of Technology, Warsaw University of Technology, Technical University of Zielona Góra, Gdynia Maritime University, Naval University of Gdynia. 3 papers were elaborated by foreign authors : from Mexico, Russia and Sweden. Employees of Alstom Power Ltd much contributed to the Symposium, and presence of representatives of two Polish firms : Polteknik and Diagnostyka Maszyn could be also clearly observed.

An interesting part of the Symposium was Round Table Discussion on :

"*Turbine Industry and Energetics Dilemmas* (*efficiency, reliability, diagnostics, control*)"

A very attractive accent of the scientific meeting was the trip to Władysławowo, a Baltic port, where the Symposium's participants had the occasion to visit a gas heat-generating plant. The modern object built in 2003 takes natural gas, through the longest-in-Europe underwater pipeline, from a gas production rig 82 km distant offshore.

Prediction of corrosion fatigue crack propagation life for welded joints under cathodic potentials

Marek Jakubowski
Gdańsk University of Technology

ABSTRACT

Enhancement of corrosion fatigue crack growth rates by cathodic protection is observed below the optimum applied potential of the protection. An empirical formula for the effect of the protective potential below -0.8 V (Ag/AgCl$_2$) on the crack growth rates for some classes of shipbuilding steels tested in salt water has been derived for medium and high value ranges of the stress intensity factor. For the lower value range the formula reflects a relatively steep decrease of the crack growth rates (against the same values in air) along with decreasing the stress intensity factor range. A simple formula for the corrosion fatigue crack propagation life under cathodic potential has been derived for fillet welded joints in bending by integrating the corrosion fatigue kinetic characteristics. The new formula for the stress intensity factor range has been used for the bent joint. The predicted "S-Np" curves have been compared with experimental data, taken from literature, for two different values of both applied potential and the plate thickness. The predicted curves correspond approximately to lower bounds of the test results. The presented procedure can be applied to joints of higher strength steels (of the yield strength σ_Y = 315 and 355 MPa) fatigued at any applied cathodic potential below -0.8 V under sea loading of (0.05÷0.2 Hz) frequency at (0÷0.2) stress ratios.

Keywords : corrosion fatigue, shipbuilding steel joints, cathodic protection

INTRODUCTION

One of the main aims of fatigue investigations is to create fatigue life calculation procedures for structural members. In the paper [1] this author presented a simple procedure for joints fatigued in air and verified it by using fatigue test results for notched steel specimens. The specimen geometry in the notch region simulated that of fillet welded joint. In the author's paper [2] the "S-N_p" curves calculated by using the procedure were compared with the fatigue test results for real fillet welded joints. The procedure gave rather conservative prediction of the total fatigue life, except for the largest values of the stress concentration factor K_t , and the longest life region (above $1\div3\times10^6$ cycles), hence it can be recommended for approximate fatigue life predictions. However, real fatigue life of ship and offshore structures is usually affected by marine environment. A prediction procedure of corrosion fatigue crack initiation life and total life for welded joints under free corrosion conditions was presented elsewhere [3].

There is a common opinion that cathodic protection increases corrosion fatigue strength and restores true fatigue limit, although the real magnitude of this effect is not certain. Some tests of notched steel specimens [4 ÷ 6] have shown that the strength in salt water under cathodic protection is higher than in air, however, other tests [7 , 8] have shown that the strength is lower than in air. Therefore the "S-N_p" curve in air cannot be always considered as conservative one for cathodically protected structures in salt water. Hartt and Hooper [5 , 6] have asserted that the fatigue limit for the protected specimens is controlled by hydrogen embrittlement and the cathodic-deposit-induced crack closure effect. Hydrogen embrittlement is well known as a crack-growth-rate accelerating process. Crack closure phenomenon leads to reduction of the crack growth rate by reduction of an effective value of the stress intensity factor that is considered to be the true crack-driving parameter. Thus they are competitive processes. However, the deposits formation process within the crack and their interaction with the crack walls is complex and practically unpredictable. The kind of the mentioned crack closure affects especially propagation of short cracks that is usually considered as a dominating part of a conventional crack initiation period. It makes the prediction of the crack initiation life for cathodically protected joints practically impossible at present. Therefore this paper deals only with the prediction of the corrosion fatigue crack propagation life N_p for welded joints under cathodic protection. The predicted "S-N_p" curves were compared with experimental data evaluated by Vosikovsky *at al.* [8] for the welded fillet joints schematically shown in Fig.1.

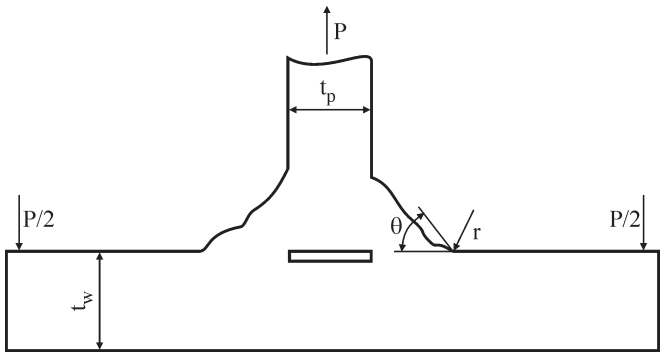

Fig. 1. *Geometry of the analyzed welded joints*

CORROSION FATIGUE CRACK GROWTH RATE CHARACTERISTICS

Fig.2 shows the effect of the applied cathodic potential Φ on the ratio β_{cat} (at $\Delta K = 20 \div 40$ MPa$\sqrt{m}$) of the crack growth rate $(da/dN)_\Phi$ at the applied potential Φ, and the crack growth rate $(da/dN)_{air}$ in air for BS4360-50D steel (σ_Y=360 MPa) [9], as well as for St41U5 steel (σ_Y = 316 MPa) and St41E-TF32 steel (σ_Y = 318 MPa)[10, 11].

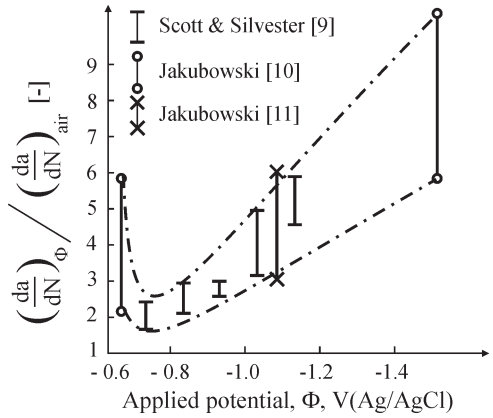

Fig. 2. *The ratio $\beta_{cat} = (da/dN)_\Phi/(da/dN)_{air}$ versus the applied potential Φ for BS4360-50D steel, acc.to [9], and for St41U5 steel and St41E-TF32 steel, acc. to [10,11]*

For $\Phi \le$ - 0.8 V (Ag/AgCl) the crack growth rate $(da/dN)_\Phi$ can be approximated by the following formula [10] :

$$\left(\frac{da}{dN}\right)_\Phi = \beta_{cat}\left(\frac{da}{dN}\right)_{air} = A\left(\frac{da}{dN}\right)_{air} \cdot (E_{free} - \Phi) \quad (1)$$

where :

E_{free} - free corrosion potential

A - coefficient of the applied cathodic potential effect.

A equals 12.2 V^{-1} for the upper envelope of the results, and 7 V^{-1} for their lower envelope; and the mean value – about 9.6 V^{-1}. Approximate values of A, evaluated by this author for a higher strength steel (σ_Y=370 MPa) at ΔK=25÷35 MPa$\sqrt{m}$ on the basis of the test results [12] are 3 ÷ 14 V^{-1}, i.e. they are of the same order as the above mentioned values.

Some tests results [9 ÷ 14] showed that the strongest enhancement of the crack growth rate by hydrogen embrittlement for steels under cathodic protection occurs approximately for ΔK above 20 MPa$\sqrt{m}$. Another set of data [7] leads to the same conclusion. The above is true for the loading frequencies f = = 0.1 ÷ 0.2 Hz and the stress ratios R = 0 ÷ 0.2. Therefore it is assumed that the crack growth rate at any applied potential $\Phi \le$ - 0.8 V and for $\Delta K \ge$ 20 MPa$\sqrt{m}$ is given by the equation (1) with A = 9.6 V^{-1}. For $\Delta K <$ 20 MPa$\sqrt{m}$ hydrogen embrittlement is not so dangerous as for ΔK values greater than 20 MPa$\sqrt{m}$, and in this case the crack growth rate quickly drops to the values observed in air, or below them. It is *ad hoc* assumed that $(da/dN)_{air}=(da/dN)_\Phi$ for $\Delta K = \Delta K_0$. Value of ΔK_0 corresponds to the end of conventional crack initiation stage and to the beginning of conventional propagation stage [1 ÷ 3]. Fig.3 schematically shows the assumed corrosion fatigue crack propagation characteristics.

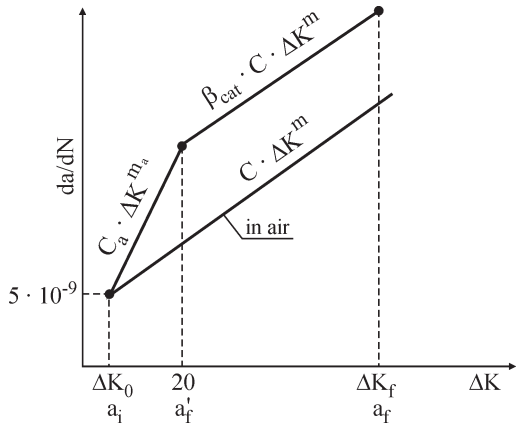

Fig. 3. *Schematic diagram of the assumed corrosion fatigue crack growth characteristics under cathodic potentials*

STRESS INTENSITY FACTOR

The stress intensity factor range ΔK was evaluated by using the formula :

$$\Delta K = \Delta S \sqrt{\pi a} \cdot Y(a / t_w) \quad (2)$$

In the present calculations, and in [1 , 2] as well, the following form of the correction function Y was assumed :

$$Y = \gamma \cdot (a/t_w)^{-\delta} \quad (3)$$

For smooth beam in bending : Y = 1.12 for $a/t_w \approx 0$ and $a/t_w = 0.305$. For notched beam the following values were assumed : $Y(0.000305) = 1.12K_t$ and $Y(0.305) = 1.12$, that led to the following equations :

$$\delta = \frac{\log(K_t)}{3} \quad (4)$$

$$\gamma = 1.12\ (0.305)^{\delta} \quad (5)$$

The stress concentration factor for the joint shown in Fig.1 was calculated by the following formula [15] :

$$K_t = 1 + 0.512\ \theta^{0.572}\ (t_w/r)^{0.469} \quad (6)$$

The values of Y calculated by using the above given formulae are comparable [2] to those evaluated by Niu and Glinka [15] by means of the finite element method.

THE ASSUMED CHARACTERISTIC CRACK LENGTHS

Values of a_i are usually – by a convention – assumed equal to 0.5 ÷ 1mm. In this paper, as well as in [1 , 2], a_i values – by another convention – correspond to a fixed value of $\Delta K = \Delta K_0$, where ΔK_0 corresponds – by an *ad hoc* assumption – to the end of the near threshold propagation rate ($da/dN=5\times10^{-9}$ m/c). Values of a_i were calculated by means of the formula :

$$a_i = \left(\frac{\Delta K_0}{\pi^{1/2}\gamma \cdot (t_w)^{\delta}\Delta S} \right)^{1/0.5-\delta} \quad (7a)$$

$$a_i \le 0.0014 \text{ m} \tag{7b}$$

The final crack length is assumed $a_f = 0.4t_w$, i.e. the same as in [2] for similar welded joints fatigued in air. The value of a_f' was evaluated from the intersection of the adjacent segments of the corrosion fatigue crack growth rate characteristics (Fig.3), i.e. by the following equation :

$$a_f' = \left(\frac{20}{\pi^{1/2}\gamma \cdot (t_w)^{\delta} \Delta S} \right)^{1/(0.5-\delta)} \tag{8}$$

CORROSION FATIGUE CRACK PROPAGATION LIFE

Integration of the assumed crack growth rate characteristics (Fig.3) leads to the following formula :

$$N_p = \frac{(a_f')^{\alpha_a} - (a_i)^{\alpha_a}}{C_a \alpha_a (\pi^{1/2}\gamma \cdot (t_w)^{\delta} \Delta S)^{m_a}} + \frac{(a_f)^{\alpha} - (a_f')^{\alpha}}{\beta_{cat} C\alpha (\pi^{1/2}\gamma \cdot (t_w)^{\delta} \Delta S)^{m}} \tag{9}$$

where :

$$\alpha_a = 1 - m_a (0.5 - \delta)$$
$$\alpha = 1 - m (0.5 - \delta)$$
$$C_a = 5 \cdot 10^{-9} \Delta K^{m_a}$$
$$m_a = \frac{\log\left(\frac{\beta_{cat} C 20^m}{5 \cdot 10^{-9}} \right)}{\log\left(\frac{20}{\Delta K_0} \right)}$$

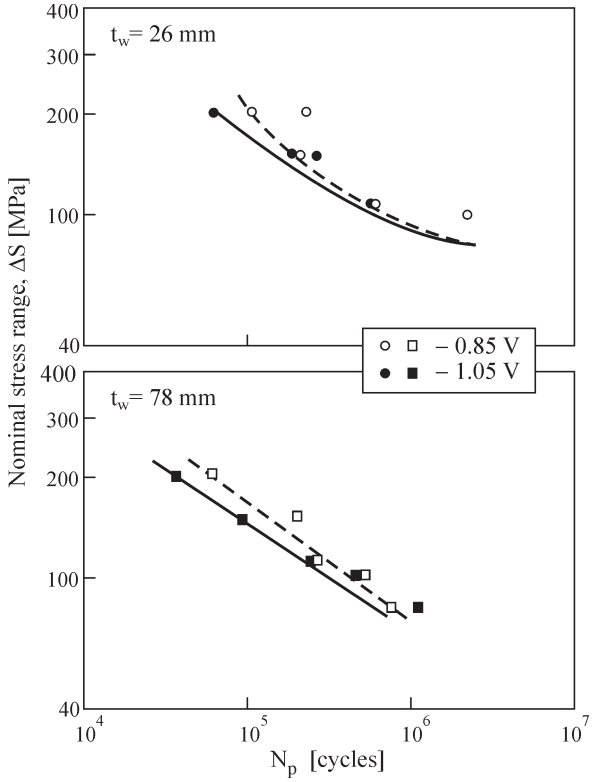

Fig. 4. *Comparison of the corrosion fatigue crack propagation curves,* "S-Np" *, acc. to equation (9) with the tests results published in [8] (here shown as the points)*

In Fig.4 corrosion fatigue lives of the welded joints shown in Fig.1, predicted by the above given formula, are compared to the lives of the same joints, determined empirically by Vosikovsky *at al*. [8] for two values of the applied cathodic potential. In order to evaluate the crack propagation life N_p obtained by Vosikovsky the crack initiation life N_i was subtracted from the total life, both read off from the appropriate figures in [8]. Values of N_p , especially those for t_w = 26 mm, demonstrate rather large scatter ; it can be partly due to the reading-off errors. The predicted "S-N_p" curves give a conservative assessment as they approximately correspond to the lower bounds of the test results, although for thicker joints such prediction is only slightly conservative.

SUMMARY

- A procedure for conservative prediction of the corrosion fatigue crack propagation life N_p of cathodically protected welded steel joints was presented. The procedure has limited applicability – it can be applied to joints manufactured of higher strength steels (of class E315 and E355, denoted by IACS as AH32, DH32, EH32, AH36, DH36, and EH36) fatigued at any applied potential lower than - 0.8 V (Ag/ /$AgCl_2$) under sea wave loading of frequencies within the range of 0.05 ÷ 0.2 Hz and stress ratios R ≈ 0 ÷ 0.2.
- The predictions for joints of steels of lower strength classes at any higher loading frequency and R values are expected to be more conservative, whereas for steels of higher classes (E390 or higher) at a lower frequency and R values it should be expected that the procedure can overestimate the crack propagation life of the joints.
- Residual welding stresses were not considered.
- The final expression for N_p concerns fillet welded joints in bending, however, the procedure can be applied to every welded joint geometry for which it is possible to calculate the stress intensity and the stress concentration factors.

NOMENCLATURE

a	–	crack length
a_f	–	final crack length, [m/cycle = m/c]
a_i	–	initial crack length, [m/c]
A	–	coefficient of the applied cathodic potential effect
c	–	cycle
C	–	material constant in the Paris equation, [m · (MPa $\sqrt{m}$)^m]
C_a	–	material constant in the Paris equation for region I under cathodic protection, [m · (MPa $\sqrt{m}$)^m]
$\left(\frac{da}{dN}\right)_{air}$	–	fatigue crack growth rate in air, [m/c]
$\left(\frac{da}{dN}\right)_{\Phi}$	–	corrosion fatigue crack growth rate under cathodic potential Φ, [m/c]
E_{free}	–	free corrosion potential, [V](Ag/$AgCl_2$)
ΔK	–	range of stress intensity factor , [MPa $\sqrt{m}$]
ΔK_f	–	final stress intensity factor, [MPa $\sqrt{m}$]
K_t	–	stress concentration factor, [-]
m	–	exponent in the Paris equation in air, [-]
m_a	–	exponent in the Paris equation for region I under cathodic protection, [-]
N	–	fatigue life, [cycles]
N_p	–	crack propagation life, [cycles]
P	–	loading force, [kN]
r	–	weld toe radius, [m]
R	–	stress ratio (= S_{min}/S_{max}), [-]
S	–	nominal stress, [MPa]
ΔS	–	nominal stress range, [MPa]
t_p , t_w	–	thickness of joined plates, [m]
Y	–	correction factor in the formula for stress intensity factor, [-]
α, α_a	–	functions appearing in eq.(9), [-]

β_{cat} – coefficient of cathodic potential effect on crack growth rate, [-]
γ – constant in eq. (3) [-]
δ – exponent in eq.(3) [-]
σ_y – yield point stress, [MPa]
Φ – cathodic potential, [V] ($Ag/AgCl_2$)
θ – weld toe angle, [radian]
IACS – International Association of Classification Societies

BIBLIOGRAPHY

1. M. Jakubowski: *Fatigue crack initiation and propagation in notched steel*(in Polish). Marine Technology Transactions, 1994, Vol.5
2. M. Jakubowski : *An approach to fatigue life calculation for non-load carrying fillet welded joints in bending*. Schiffbauforschung, 1995, Vol.34, No.2/3
3. M. Jakubowski: *A procedure to corrosion fatigue life prediction for fillet welded joints under free corrosion conditions.* Proc. 2nd Int. Conf. Environmental Degradation of Engineering Materials EDEM'2003. Bordeaux, France. June 29-July 2, 2003
4. L.A. Glikman, Yu.E. Zobaczew : *O wozmożnosti zaliecziwania ustałostnych trieszczin w procesie ustałosti* (in Russian) In: *Problemy procznosti i płasticznosti twiordych tieł*. Publ.: Nauka (Science). 1979
5. W.C. Hooper, W.H. Hartt: *The influence of cathodic polarisation upon fatigue of notched structural steel in sea water*. Corrosion, 1978, No.9
6. W.H. Hartt, W.C. Hooper: *Endurance limit enhancement in 1018 steel in sea water: specimen size and frequency effects.* Corrosion. 1980, No.3
7. R.P. Gangloff: *Corrosion fatigue crack propagation in metals*. Environment Induced Cracking of Metals. Publ: NACE (National Association of Corrosion Engineers). Houston. 1990
8. O. Vosikovsky, R.Bell, D.J.Burns, U.H.Mohaupt: *Thickness effect on fatigue life of welded joints - revue of the Canadian program.* 8th Int. Conf. Offshore Mechanics and Arctic Engineering. Publ. ASME (American Society of Mechanical Engineering). 1989, Book No.10285C
9. P.M. Scott, D.R.V. Silvester : *The influence of seawater on fatigue crack propagation in structural steel.* Department of Energy, UK OSRP (United Kingdom, Offshore Steel Research Project). Technical Report, 1975, No.3/03
10. M. Jakubowski : *Influence of cathodic potential on the fatigue crack growth rate for ordinary shipbuilding steel in salt water.* 9th Int. Colloquium on Mechanical Fatigue of Metals. Smolenice, CSSR. December 1987
11. M. Jakubowski: *Fatigue and corrosion fatigue crack growth rates for two new shipbuilding steels* (in Polish). Marine Technology Transactions, 1993, Vol.4
12. M. Murakami, W.G. Ferguson: *The effect of cathodic potential and calcareous deposits on corrosion fatigue crack growth rate in seawater for two offshore structural steels.* Fatigue & Fracture of Engineering Materials & Structures. 1987, Vol.9
13. O. Vosikovsky: *Fatigue crack growth in an X65 line pipe steel at low cyclic frequencies in aqueous environments.* Journal Engineering Materials and Technology. 1975, Vol.97
14. Yu.R. Brook, J. Cole, D. Morabites, G. Demofonti:*The effect of cathodic protection potential on corrosion fatigue crack growth rate of an offshore structural steel*. Fatigue & Fracture of Engineering Materials & Structures. 1996, Vol.19
15. X. Niu, G. Glinka : *The weld profile effect on stress intensity factor in weldments.* International Journal Fracture. 1987, Vol.36.

CONTACT WITH THE AUTHOR

Marek Jakubowski, D.Sc., Eng.
Faculty of Ocean Engineering
and Ship Technology,
Gdańsk University of Technology
Narutowicza 11/12
80-952 Gdańsk, POLAND
e-mail : marjak@pg.gda.pl

Conference

ITEM 2004

POMERANIAN SCIENTIFIC CONFERENCE

Beginning from 1996, serial scientific conferences on materials engineering have been organized by Materials Engineering Department, Mechanical Faculty, Gdańsk University of Technology. In them have participated scientific workers and experts in this area acting in northern Poland, and invited guests cooperating with scientifc centres of the region.

The Conferences are held under auspices of Pomeranian Division, Polish Society of Materials Technology. They are aimed at giving review of scientific and technological development, exchange of experience, planning common undertakings etc.

4th such Conference, titled :

***Materials Engineering* – ITEM 2004**

was held at Bychowo near Gdańsk on 19÷21 May 2004.

During the Conference were presented and discussed 49 papers prepared by specialists from 11 scientific research centres including Hungarian Academy of Sciences, Budapest.

To the Conference program
most contributed scientific workers of :

- Gdańsk University of Technology
  (22 papers of single authors + 9 of co-authors)
- Gdynia Maritime University (4 + 4)
- Koszalin Technical University (5 + 1)
- Ship Design & Research Centre, Gdańsk (2 + 2)
- Technical University of Szczecin (2 + 0)
- Institute of Fluid-Flow Machinery, Gdańsk (0 + 3).

Combustion in Piston Engines

Technology ∗ Evolution ∗ Diagnoses ∗ Control

A very inspiring book written by Prof. Antoni K. Oppenheim of University of California, has been recently published by Springer-Verlag Berlin Heidelberg New York (marked ISBN 3 - 540 - 20104 - 1).

As the title of the book suggests it concerns the technology of combustion in internal combustion engines - the prime automotive powerplant today. The problem is important because of the escalating emission of pollutants by combustion and the dwindling natural resources of energy. As a consequence, the automotive industry found itself confronted with a significant amount of societal pressures and governmental regulations, which brought about a state of flux and confusion.

Confronted with the mounting dissatisfaction with current technology of internal combustion engines, the automotive industry is involved nowadays in a frantic search for alternative fuel and alternative energy conversion systems. The question how much effort should be spent on searching for an alternative system, while the attractive prospects of equivalent progress in the technology of combustion in piston engines are disregarded, is open.

The purpose of the book – its author says in Preface – is to provide the background for implementation of such a progress. This is accomplished by providing an assessment of the technology of combustion in piston engines, followed by furnishing an engineering method of approach for evaluation of the effectiveness with which fuel is utilized in the engine cylinder, and demonstrating how it can be improved.

These subjects are exposed, respectively, in two parts :

Part 1 made of :

Ch. 1. : **Overview**, describing what the technology of combustion in piston engines is all about
Ch. 2. : **Perspective**, providing an account of how did it got to its present state
Ch. 3. : **Prospective**, pointing out how it technology can be advanced and what gains can be thereby derived

Part 2 is based on the recognition that combustion is at the heart of a piston engine (hence chapters of this part are entitled in medical terms)

Ch. 4 : **Diagnosis** introduces the principles of a "engine cardiology" profession
Ch. 5. : **Procedure** prescribes the manner in which it is applied to a given engine
Ch. 6. : **Prognosis** provides an insight into its prospects.

In the author's opinion the technology of combustion in piston engines is today at the threshold of a quantum leap, comparable to that which took place in electronics by its transition from vacuum tubes to transistors, and that his book provides a recipe for advancement of the technology in question.

Engines of the future, based on this advancements, would feature distributed combustion executed by means of Pulse Jet Injection and Ignition (PJI&I) actuators modulated by Micro-Electronically Controlled Combustion Systems (MECC) in response to signals provided by pressure sensors to assess the effectiveness with which fuel is utilized in an engine cylinder, and to monitor the operation of MECC system in optimizing the performance of a PJI&I system.

The book suggests that by the use of these systems it would be possible to build a car engine for which the formation of pollutants can be reduced by orders of magnitude, while the consumption of fuel is halved.

The book, written in a very clear and concise way, consists of 160 pages and includes many figures and diagrams and a dozen or so reference sources.

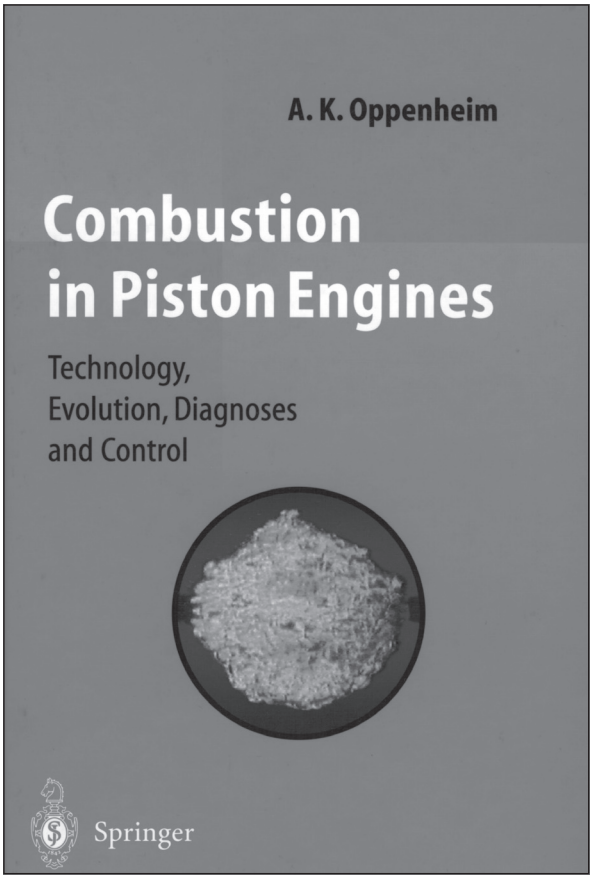

Application of statistical methods and artificial neural networks for approximating ship's roll in beam waves

Tomasz Cepowski
Maritime University of Szczecin

ABSTRACT

In the paper, were presented approximations of numerical calculations of ship's roll on the basis of main service parameters of the ship. This way were obtained several relationships which make it possible to approximate ship roll in regular and irregular waves by using the parameters available in the phase of voyage routing. The relationships were elaborated by means of artificial neural networks as well as linear and non-linear regression methods. A comparative analysis of the methods regarding approximation accuracy against standard data was also performed.

Keywords : ship's roll, regular wave, irregular wave, approximation, neural networks, regression methods

INTRODUCTION

Within the contemporary shipping problems there is a problem of searching for ship voyage route satisfying several criteria among which the following usually are the most important :

- voyage duration time (at assumed parameters of ship propulsion system)
- operational cost which mainly depends on fuel consumption.

A limitation which seriously influence route choice is the condition of safe shipping, which consists of many factors among which ship's behaviour in rough seas should be distinguished.

So many parameters influence ship's behaviour in waves that accounting for all of them makes the voyage routing process very complicated. Hence, out of all the parameters, ship master is forced to take into account only most important ones, among which wave parameters, ship's motion parameters or also selected hydromechanical parameters of the ship, are numbered. The small amount of available information does not make it possible to use exact methods of determination of ship motion in waves.

In the subject-matter literature, methods making it possible to solve the problem in a satisfactory way, are still lacking. Design recommendations dealing with ship seakeeping qualities, given in classification rules, are of a very limited character. The calculation procedures there presented are rather inaccurate and they allow to determine only „designed" ship motion amplitudes and accelerations which are connected only to a certain degree with real ship behaviour in waves. The approximations of ship seakeeping qualities published in the scientific literature are too general, rather inaccurate, and usually applicable only to a given hull form [1,5].

In this paper an attempt to solve the problem has been undertaken, aimed at elaboration of a simplified but exact model of predicting ship's roll on the basis of main ship service parameters.

METHOD

The research in question was limited to approximation of ship's roll in regular and irregular waves coming from the direction perpendicular to ship's plane of symmetry. It was assumed that approximations of the oscillations have to be elaborated on the basis of the parameters taken into account in ship voyage routing and simultaneously having significant influence on the motions. Among such parameters the following are usually numbered :

- wave parameters in the form of its height and period (in the case of aproximation of ship roll in irregular waves)
- ship motion parameters
- ship service parameters associated with, a.o., ship mass distribution and its hull hydrostatic characteristics.

In the research in question it was adopted an approach of approximating the standard values of the roll angles ϕ (determined by means of exact numerical methods) by using the approximating function *f* on the basis of the n-element set of input parameters $W[X_1, X_2, ... X_n]$:

$$\phi = f(W) \tag{1}$$

where :

W - n-element set of input parameters : $X_1, X_2, ... X_n$
ϕ - standard values of roll angles calculated by means of the exact method
f - approximating function searched for.

STANDARD VALUES OF ROLL ANGLES

Standard values of roll angles were determined by using exact numerical methods based on the two-dimensional flow theory, i.e. the SEAWAY software (was elaborated by Shiphydromechanics Laboratory, Delft University of Technology, The Netherlands) which calculates ship motions in regular and irregular waves. In Fig.1 are presented the ship roll amplitude characteristics calculated by means of the software, and showed together with the characteristics obtained from model tests [10].

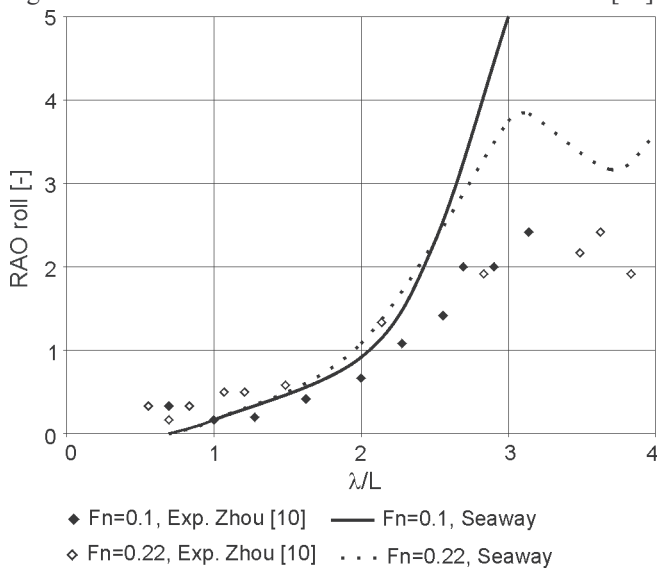

Fig. 1. *Roll angle amplitude characteristics of the containership „Nedlloyd Dejima" of : L = 270 m, B = 32.20 m, d = 10.85 m, C_B = 0.596, Z_G = 16.45 m, in beam waves, acc. [10]*

The approximations and numerical calculations were carried out for the S-175 model containership of the following main dimensions :

L (length between perpendiculars) = 175 m
B (breadth) = 25.4 m
d (design draught) = 9.5 m.

Its hull form is given in Fig.2.

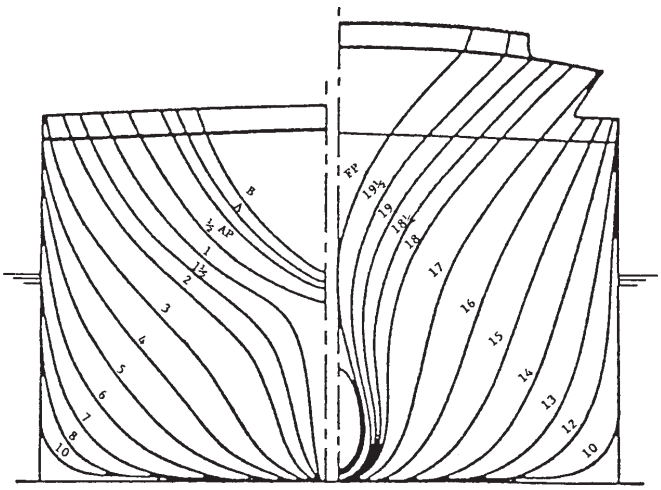

Fig. 2. *Theoretical hull frames of S-175 containership, acc. [4]*

The numerical calculations were performed by applying, a. o., the modified method of two-dimensional flow, accounting for diffraction of wave loads [4] , and assuming ITTC wave spectrum.

On the basis of literature data, were selected the parameters which have decisive influence on ship roll, and simultaneously considered as the service ones. To them it belongs, a.o. :

- ⇨ the ship volumetric displacement ∇
- ⇨ the initial transverse metacentric height GM
- ⇨ the height of the ship gravity centre Z_G.

Taking into account that the volumetric displacement ∇ can be expressed in the form of the mean draught *d* , and that the initial transverse metacentric height GM depends on the height of ship gravity centre Z_G, one decided to determine the ship roll approximations by using :

- ★ the mean draught d
- ★ the initial metacentric height GM

for which the following ranges of their values were assumed :

- ⅄ for d : from 7 to 9 m
- ⅄ for GM : from 0.3 to 1.5 m

and

- ⅄ for the ship speed V : from 0 to 20 knots.

Additionally, for approximation of ship roll in irregular waves it was assumed :

- ❋ values of the significant wave height Hs : from 2 to 4.5 m, taken with 0.5 m step
- ❋ values of the characteristic wave period T : from 6.5 to 14.5 s, taken with 2 s step.

For all the above mentioned variants roll angle amplitudes of ship in regular and irregular waves were calculated, and this way the set of standard data for approximations was obtained.

APPROXIMATION OF ROLL AMPLITUDES OF S-175 CONTAINERSHIP IN REGULAR WAVES

The approximation of ship roll amplitudes in regular waves (in irregular waves as well) was carried out by means of statistical methods, i.e. linear and non-linear regression, as well as artifical neural networks. The latter method belongs to relatively novel mathematical-numerical methods placed in the field of „artificial intelligence", and it finds more and more applications in different domains of science and engineering. The research results published in [6, 8, 9] show broader and broader possiblities of application of artificial neural networks to the problems of ship design and operation.

On the basis of [1,8] and the performed investigations it has appeared that the best model of roll amplitude characteristics against the assumed standard data is the following :

$$Y_\phi(\omega) = \frac{a}{1-\left(\frac{\omega}{b}\right)^2} \qquad (2)$$

where :

a , b – coefficients dependent on ship service parameters
ω – wave frequency [s^{-1}].

The coefficients *a* and *b* were approximated by using the statistical methods and artificial neural networks, as shown below.

Approximation of the coefficients a *and* b *by using statistical methods*

To approximate the coefficients *a* and *b* in the equation (2) linear and non-linear regression was used. When using the linear regression the following relationships appeared the best out of all investigated models :

$$a = \alpha_0 \cdot d + \alpha_1 \cdot GM + \alpha_2 \cdot d^2 + \\ + \alpha_3 \cdot \frac{GM}{d} + \alpha_4 \cdot V + \alpha_5 \cdot GM \cdot d \quad (3)$$

$$b = \alpha_6 \cdot d + \alpha_7 \cdot \left(\frac{GM}{d} \right)^2 + \alpha_8 \cdot d^2 \quad (4)$$

where :

α_0 , ..., α_8 – coefficients whose values are given in Tab. 1
The remaining symbols – as explained above.

Table 1

α_0	α_1	α_2	α_3	α_4	α_5	α_6	α_7	α_8
0.412	4.117	-0.028	-39.160	0.314	-0.035	0.058	3.040	-0.005

When applying non-linear regression
the following relationships appeared the best ones :

$$a = \alpha_0 + \exp\left(\begin{array}{l} \alpha_1 + \alpha_2 \cdot d + \alpha_3 \cdot V + \\ + \alpha_4 \cdot GM + \alpha_5 \cdot \dfrac{GM}{d} \end{array} \right) \quad (5)$$

$$b = b_0 \cdot \beta_0 + b_1 \cdot \beta_1 \quad (6)$$

where :

$$b_0 = (\alpha_6 + \alpha_7 \cdot d + \alpha_8 \cdot V + \alpha_9 \cdot GM)$$
$$b_1 = (\alpha_{10} + \alpha_{11} \cdot d + \alpha_{12} \cdot V + \alpha_{13} \cdot GM)$$

$\beta_0 = 1$ if $b_0 \le \alpha_{14}$ otherwise $\beta_0 = 0$

$\beta_1 = 1$ if $b_1 > \alpha_{14}$ otherwise $\beta_1 = 0$

α_0 , ..., α_{14} – coefficients whose values
are given in Tab.2 and 3.

Table 2

α_0	α_1	α_2	α_3	α_4	α_5	α_6	α_7
0.9319	45.235	-5.2798	0.0676	105.41	-950.58	0.165	$2.25 \cdot 10^{-3}$

Table 3

α_8	α_9	α_{10}	α_{11}	α_{12}	α_{13}	α_{14}
$-5.46 \cdot 10^{-4}$	-0.013	0.064	-0.014	$8.339 \cdot 10^{-6}$	0.3284	0.212

Approximation of the coefficients a *and* b *by means of artificial neural networks*

Among all investigated networks used for approximating the coefficients *a* and *b* in the equation (2) the MLP neural networks of the below given form, showed the highest accuracy :

$$a, b = \frac{\left(\dfrac{1}{1 + e^{-([d, V, GM] \cdot S + P) \cdot A - B)}} \cdot C - \alpha_0 \right) - \alpha_1}{\alpha_2} \quad (7)$$

where :

the symbols : d, GM, V – as explained above.
S – the vector of normalizing values : [0.5 0.05 0.833]
P – the vector of displacement values : [- 3.5 0 - 0.250]

The matrices, vectors and constants
necessary to determine the coefficient *a* :

A – matrix of weight values :

$$\begin{bmatrix} -0.1304 & 0.8757 & -0.9335 & -0.0855 & 0.9179 & -0.0139 & 0.0338 & -0.6867 & 0.5367 & -0.3011 & 0.8537 & -0.1561 & -0.9966 \\ 0.4534 & 0.6205 & -0.7704 & -0.3399 & 0.4939 & 0.8646 & -0.7616 & 0.3134 & -0.5045 & -0.3016 & -0.3004 & 0.6048 & -0.0967 \\ 0.1259 & 0.0096 & 0.4784 & 0.9856 & 0.6298 & 0.7879 & -0.2093 & -0.5050 & -0.9623 & 0.2246 & -0.8858 & -0.2999 & -0.1227 \end{bmatrix}$$

B – vector of threshold values :

[-0.93 -0.764 0.847 -0.201 1.02 0.635 -0.568 -0.181 -0.522 0.926 1.109 -0.516 -0.863]

C – vector of weight values :

[1.03 -0.025 -0.528 -0.34 -0.469 -0.64 -0.259 -0.053 0.275 -0.588 -0.810 0.804 -0.082]

α_0, α_1, α_2 – the coefficients having the values :
α_0 = - 0.323, α_1 = - 0.305, α_2 = 0.496.

The matrices, vectors and constants
necessary to determine the coefficient *b* :

A – matrix of weight values :

$$\begin{bmatrix} 1.1072 & 2.6231 & 5.2094 & -4.4498 & 1.7052 \\ 0.5590 & 2.2139 & -1.6990 & 1.0816 & 0.8587 \\ -1.4717 & -2.6282 & -2.9165 & 0.8025 & -1.6338 \end{bmatrix}$$

B – vector of threshold values :

[-0.515 0.813 -1.374 1.575 -0.769]

C – vector of weight values :

[1.562 -1.461 -2.731 -3.637 2.197]

α_0, α_1, α_2 – the coefficients having the values :
α_0 = - 0.773, α_1 = - 0.547, α_2 = 3.475.

Assessment of the approximations

To assess accuracy of the approximations,
were used RMS values calculated from the expression :

$$RMS = \frac{1}{n} \sqrt{\frac{(Y_{\phi w} - Y_\phi)^2}{m}} \quad (8)$$

where :

RMS – error value
$Y_{\phi w}$ – standard values of ship roll amplitudes
Y_ϕ – approximated values of ship roll amplitudes
n – number of considered variants
m – number of the values approximated on the amplitude characteristics.

The accuracy analysis was carried out for :

1) values of the input parameters for which approximations were elaborated
2) the value of the initial metacentric height GM = 2 m, being out of the range of the elaborated approximations.

Values of the RMS errors regarding the elaborated relationships, for the above mentioned cases, are given in Tab.4. And, in Figs.3 to 5 the elaborated approximations are compared respective to selected variants.

Table 4

RMS error	MLP neural network	Linear regression	Non-linear regression
for the input parameters (case 1)	3.6	16.4	7.8
for GM = 2 m (case 2)	4.2	7.8	8.8

From Tab.4 and Fig.3 to 5 it results that the approximations obtained by using the MLP artificial neural network show the greatest accuracy regarding interpolation and extrapolation.

APPROXIMATION OF ROLL AMPLITUDES OF S-175 CONTAINERSHIP IN IRREGULAR WAVES

Approximations of numerically calculated significant values of roll angle amplitudes in irregular waves were performed on the basis of ship service parameters as well as wave parameters. To this end also statistical methods (linear and non-linear regression) and artificial neural networks were applied.

Explanation to Figs 3÷5 :

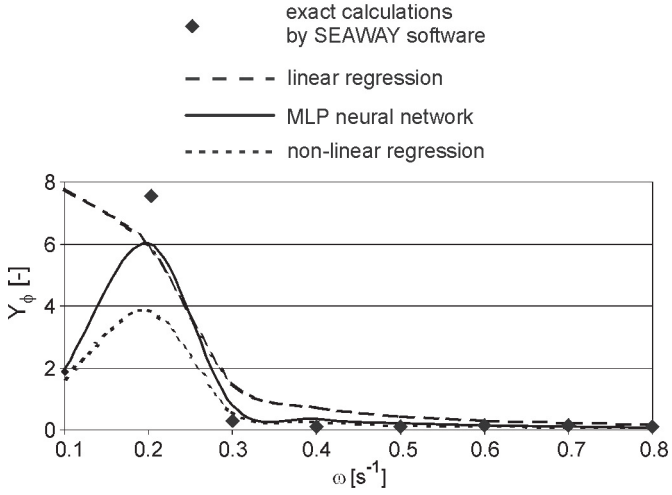

Fig. 3. *Values of the ship roll transfer function Y_ϕ, at V = 10 kts, d = 9 m, GM = 0.3 m*

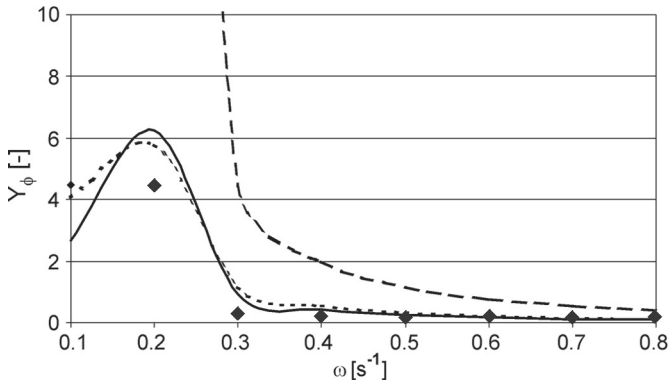

Fig. 4. *Values of ship roll transfer function Y_ϕ, at V = 20 kts, d = 7 m, GM = 0.3 m*

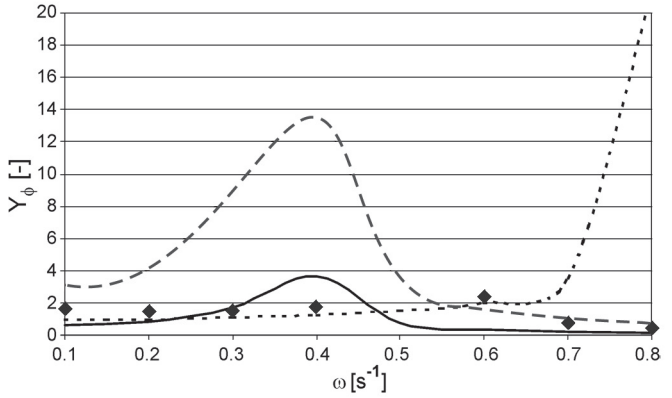

Fig. 5. *Values of ship roll transfer function Y_ϕ, at V = 10 kts, d = 8 m, GM = 2.2 m*

Approximation of ship roll amplitudes in irregular waves by means of statistical methods

When using linear regression, out of all considered relationships, the following one appeared the best :

$$\phi_{1/3} = \alpha_0 + \alpha_1 \cdot GM \cdot T \cdot Hs + \alpha_2 \cdot d \cdot GM \cdot \cdot V \cdot T \cdot Hs + \alpha_3 \cdot d^2 \cdot GM^2 + \alpha_4 \cdot GM^2 \quad (9)$$

where :

$\phi_{1/3}$ – significant roll angle amplitude [°]
α_0 , α_1 , α_2 , α_3 , α_4 – the coefficients whose values are given in Tab.5
d, GM, V – as explained above
T – characteristic wave period [s]
Hs – significant wave height [m].

Table 5

α_0	α_1	α_2	α_3	α_4
- 0.34231	0.09918	- 0.00021	0.01735	- 1.00743

And, when applying non-linear regression, the exponential relationship of the below given form appeared the best out of all considered models :

$$\phi_{1/3} = \alpha_0 + \exp\left(\begin{array}{l} \alpha_1 + \alpha_2 \cdot d + \alpha_3 \cdot GM + \\ + \alpha_4 \cdot V + \alpha_5 \cdot T + \alpha_6 \cdot Hs \end{array} \right) \quad (10)$$

where :

α_0 , α_1 , α_2 , α_3 , α_4 , α_5 , α_6 – the coefficients whose values are given in Tab.6.

Table 6

α_0	α_1	α_2	α_3	α_4	α_5	α_6
-1.37532	-1.35646	0.07263	0.85908	- 0.01607	0.04597	0.27059

In both relationships the values of the determining coefficient prove that the proposed relationships well match up with the standard data. From variance analysis it results that both equations are essential. Simultaneously the regressions of dependent variables $\phi_{1/3}$ indicate that all components of both equations (including their free terms) are essential.

Approximation of ship roll amplitudes in irregular waves by means of artificial neural networks

Out of all considered networks, the following neural networks revealed the best approximation features :

- the MLP network of 5 inputs x 11 hidden neurons x 1 output
- the RBF (Radial Basic Functions) network of 5 inputs x 180 hidden neurons x 1 output.

Statistically significant roll angle amplitudes $\phi_{1/3}$ approximated by means of the MLP neural network can be calculated with the use of the following equation :

$$\phi_{1/3} = \frac{\left(\frac{1}{1 + e^{-([d, GM, V, T, Hs] \cdot S + P) \cdot A - B)}} \cdot C - \alpha_0 \right) - \alpha_1}{\alpha_2} \quad (11)$$

where :

$\phi_{1/3}$, d, GM, V, T, Hs – as explained above

A – matrix of weight values :

$$\begin{bmatrix} 0.1387 & 0.3845 & -0.3169 & -0.1804 & -0.3674 & -0.6876 & 0.0606 & -0.3752 & 0.2717 & 0.0268 & 0.0807 \\ 0.1743 & -3.5447 & -2.1067 & -1.0170 & 0.1016 & -0.8214 & -1.3072 & 0.1762 & 3.2725 & -0.2252 & 2.8329 \\ 0.3839 & -0.9977 & 0.2728 & 0.0992 & 0.5148 & -0.2305 & -0.3881 & 1.5009 & -0.2839 & 0.6204 & 0.1285 \\ -0.4993 & 0.9608 & -1.3266 & -2.4275 & 1.0287 & -0.2497 & -3.1174 & -0.1543 & 3.1220 & -0.1918 & 3.7166 \\ 0.3733 & 0.9096 & 0.9033 & -0.2308 & 0.3956 & -0.0745 & 0.4807 & -1.1985 & 0.2697 & 0.6046 & -0.1800 \end{bmatrix}$$

B – vector of threshold values :

[0.2133 2.9327 -0.6466 -1.6343 -0.2292 0.7501 -2.5607 -1.9524 2.1205 0.9054 2.9620]

C – vector of weight values :

[0.2687 -1.7393 -1.0205 -1.7328 0.3104 0.7946 2.5177 -1.0679 -2.2512 0.7164 2.6939]

S – vector of values :

[0.500 0.833 0.050 0.125 0.400]

P – vector of displacement values :

[-3.500 -0.250 0.000 -0.813 -0.800]

α_0, α_1, α_2 – coefficients having the values :

α_0 = - 0.2061, α_1 = - 0.017, α_2 = 0.102.

To calculate values of the ship roll amplitudes $\phi_{1/3}$ approximated with the use of the RBF neural network one can apply the following generalized equations :

$$\phi_{1/3} = ([d, GM, V, T, Hs] \cdot A + B) \cdot C \qquad (12)$$

where :

A – [5 x 180] matrix of weight values
B – 180-element vector of constants
C – 180-element vector of weight values.

Input values for the equation (12) were normalized to be contained within the interval : 0...1, and the neurons of hidden layer were activated by means of an exponential function. Because of too large dimensions of the matrix A and remaining vectors it was decided not to present values of elements of the matrices and vectors as well as values of normalizing coefficients.

Values of correlation coefficients of both networks show that both proposed models well match up with standard values.

Assessment of the approximations

To assess accuracy of the approximations, RMS' values calculated from the following expression, were applied :

$$RMS' = \sqrt{\frac{(\phi_w - \phi_{1/3})^2}{n}} \qquad (13)$$

where :

RMS' – error value
ϕ_w – standard values of ship roll amplitudes
$\phi_{1/3}$ – approximated values of ship roll amplitudes
n – number of considered variants.

The accuracy analysis was carried out for :

1) values of the input parameters for which approximations were elaborated
2) the value of the initial metacentric height GM = 2 m, and that of the significant wave height Hs = 3 ÷ 6 m, being behind the range of the elaborated approximations.

Values of the RMS' errors associated with the elaborated relationships for the above mentioned cases are given in Tab.7.

Table 7

RMS' error	MLP neural network	RBF neural network	Linear regression	Non-linear regression
for the input parameters (case 1)	0.15°	0.21°	0.76°	0.83°
for the values behind the range of input parameters (case 2)	0.69°	5.32°	1.99°	2.53°

From the table it results that in both cases the most accurate appear the approximations obtained with the use of the MLP artificial neural network. The approximations elaborated by means of linear regression are loaded with a small error in the case of interpolation, and with rather large one as far as extrapolation operations are concerned.

Addtionally, to more precisely verify the proposed relationships the falsification method was applied [7]. To this end, such ranges of input parameters were searched for which the elaborated approximations appeared the least accurate. Results of the investigations are graphically presented in Fig.6÷÷8 (for interpolation), and in Fig.9 (for extrapolation). The diagrams confirm that in both cases the approximation with the use of the MLP artificial neural network appears the most accurate.

Explanation to Figs 6÷9 :

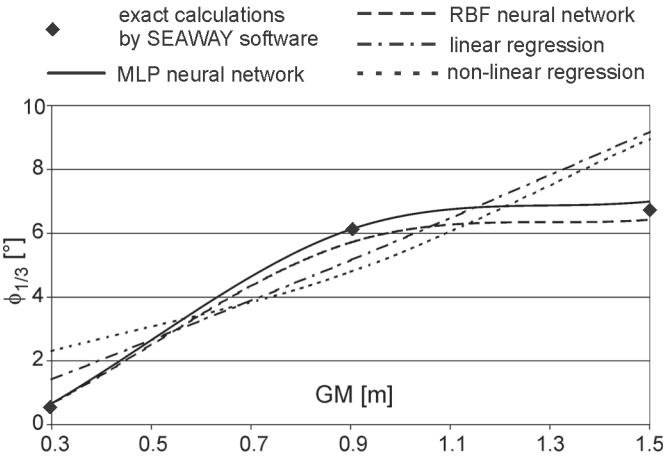

Fig. 6. *Significant ship roll amplitudes $\phi_{1/3}$, at GM = var , d = 7 m , V = 0 , T = 14.5 s , Hs = 4 m.*

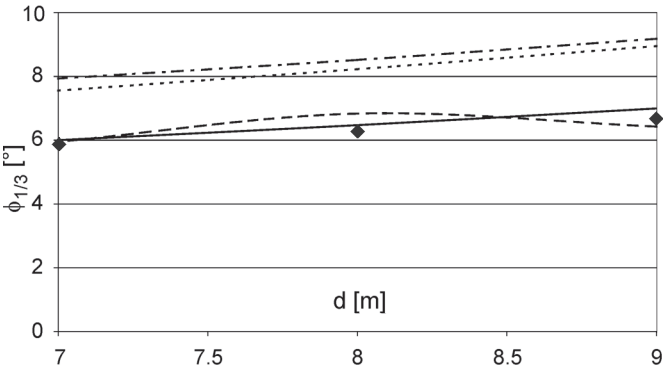

Fig. 7. *Significant ship roll amplitudes $\phi_{1/3}$, at d = var , GM = 1.5 m , V = 0 , T = 14.5 s , Hs = 4 m*

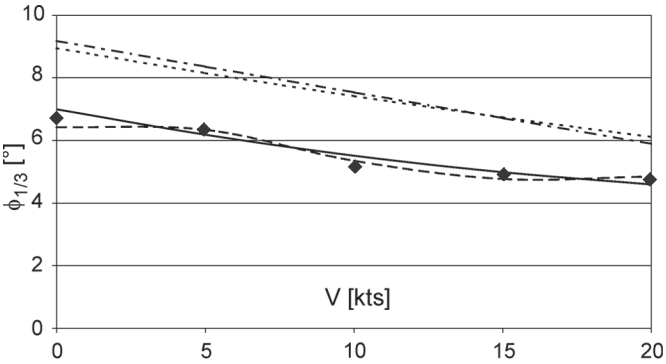

Fig. 8. *Significant ship roll amplitudes $\phi_{1/3}$, at V = var , d = 9 m , GM = 1.5 m , T = 14.5 s , Hs = 4 m*

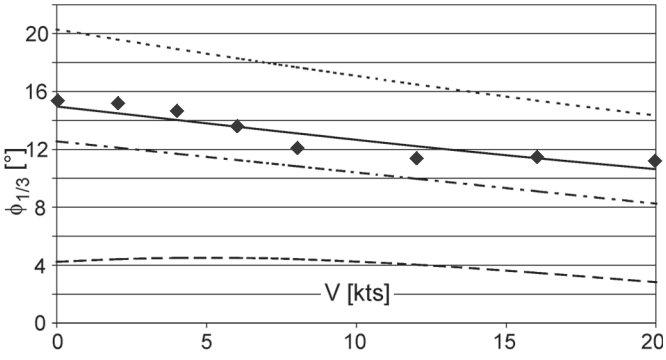

Fig. 9. *Significant ship roll amplitudes $\phi_{1/3}$, at V = var , d = 9 m , GM = 2 m , T = 9.5 s , Hs = 6 m*

ACCURACY ASSESSMENT OF THE ELABORATED APPROXIMATIONS WITH A VIEW OF PREDICTING SHIP ROLL IN IRREGULAR WAVES

The above presented relationships make it possible to approximate ship roll in regular and irregular waves. The first method allows to approximate roll amplitude characteristics on the basis of the ship service parameters (d, GM, V) and next to calculate any statistical values of roll amplitudes for any wave spectrum. And, the second method makes it possible to directly approximate ship roll amplitudes in irregular waves.

In this part of the investigations the two approaches were compared regarding their accuracy in predicting ship roll motion in irregular waves against the standard values. The analysis was performed on assuming the values of input parameters to be contained within :

- ❖ the ranges of the parameters for which the approximations were elaborated
- ❖ behind the ranges of the parameters, in order to test this way extrapolation capabilities of the elaborated relationships.

In the first case the calculations were carried out for :
d = 8 m GM = 0.9 m Hs = 4 m.
And in the second case for :
d = 9.5 m GM = 2 m Hs = 6 m.

In both cases the characteristic wave period T was assumed equal to10 s, and the ship speed V within the range from 0 to 20 knots.

The analysis was performed for the approximations whose accuracy was the greatest and which were described by :

- ➢ for ship roll in regular waves – the relationship (2) having the coefficients approximated with the use of (3), (4), and (7)
- ➢ for ship roll in irregular waves – the relationships (9) and (11).

In order to determine ship roll in irregular waves the expression (2) and the wave energy spectrum recommended by ITTC was used. Results of the calculations are graphically presented in Fig.10 and 11.

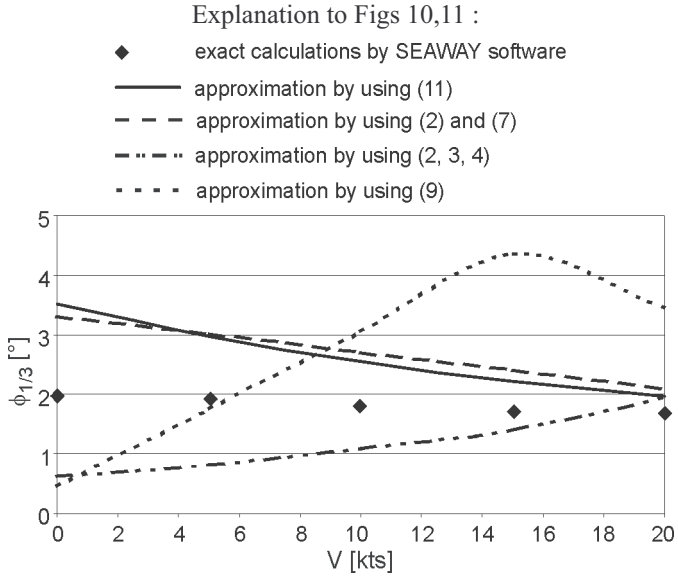

Fig. 10. *The significant ship roll amplitudes $\phi_{1/3}$, at V = var , d = 8 m , GM = 0.9 m , H = 4 m , T = 10 s*

From the diagrams given in Fig.10 and 11 it results that both presented approaches show similar interpolation capabilities. The extrapolation of roll amplitudes in irrerular waves by using (9) and (11) yields rather accurate results against the standard values. Whereas the application of the approximation (2) to determine significant roll amplitudes in irregular waves brought in erronous solutions, especially in the case of extrapolation.

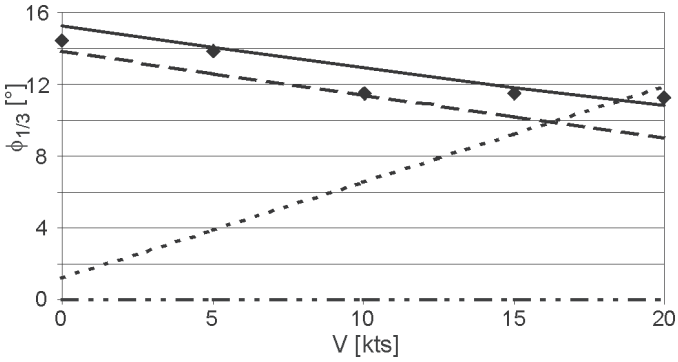

Fig. 11. *The significant ship roll amplitudes $\phi_{1/3}$, at V = var , d = 9.5 m , GM = 2 m , H = 6 m , T = 10 s*

RECAPITULATION

- ❍ In the paper were presented approximations of ship roll in regular and irregular waves by means of artificial neural networks and linear and non-linear regression methods, on the basis of main ship service parameters (speed, draught, initial transverse metacentric height), and – in the case of approximation ship roll in irregular waves – wave parameters (significant height and characteristic period of waves). The example approximations were elaborated for S-175 model containership.
- ❍ From the performed investigations it results that the relationships obtained by means of MLP artificial neural networks show the largest accuracy regarding interpolation and extrapolation of ship roll amplitudes both in regular and irregular waves.
- ❍ Next, basing on the above mentioned approximations, two approaches to predicting ship roll amplitudes in irregular waves were analyzed :
  - ♦ approximation of roll amplitudes in regular waves, and next calculation of their significant values in irregular waves
  - ♦ direct approximation of roll amplitudes in irregular waves.
- ❍ From the performed investigations it results that the approximation of ship roll angles by means of amplitude characteristics yields satisfactory results only in the case of interpolation. Whereas the second approach provides relatively accurate solutions both in the case of interpolation and extrapolation.
- ❍ The presented method makes it possible to approximate ship roll angle amplitudes calculated by using exact numerical methods, and they can be also applied to determine optimum ship voyage routes. The proposed approach may be also used to approximate real values of roll angle amplitudes on the basis of data recorded onboard the ship during its service.

NOMENCLATURE

B - ship breadth
C_B - block coefficient
d - ship draught
F_n - Froude number
GM - initial transverse metacentric height

H_s - wave height
L - ship length between perpediculars
T - characteristic wave period
V - ship speed
Z_G - height of the ship gravity centre
∇ - ship volumetric displacement
λ - wave length
ϕ - roll amplitude
ω - wave frequency

Akcronyms

ICLL - International Convention on Load Lines
MLP - Multilayer Perceptron
RAO - Response Amplitude Operator
RBF - Radial Basic Functions
UBS - Universal Bulk Cargo Ship

BIBLIOGRAPHY

1. Cepowski T: *The Proposal of Optimization Method of Ships Design Parameters on The Basis of Short-Term Rolling Prediction*. 13th International Conference on Hydrodynamics in Ship Design, HYDRONAV'99, Gdańsk-Ostróda. 1999
2. Calisal S.M., Howard D., Mikkelsen J.: *A Seakeeping Study of the UBS Series*. Marine Technology, Vol. 34, No.1, Jan. 1977
3. Journée J.M.J.: *Verification and Validation of Ship Motions Program SEAWAY*, Report1213a. Delft University of Technology, The Netherlands. 2001
4. Journée J.M.J.: *Theoretical Manual of SEAWAY*. Report1216a, Delft University of Technology, The Netherlands. 2001
5. Kukner A., Aydm M.: *Influence of Design Parameters on Vertical Motions of Trawler Hull Forms in Head Seas*, Marine Technology, Vol. 34, No.3, July 1997
6. Mesbashi E., Bertram V.: *Empirical Design Formuale Using Artificial Neural Nets*. 1st International EuroConference on Computer Applications and Information Technology in the Maritime Industries, COMPIT'2000. Potsdam. 2000
7. Popper K.: *The Logic of Scientific Discovery*. Routledge, 14th Printing. 1977
8. Szelangiewicz T., Cepowski T.: *Application of Artificial Neural Networks to Investigation of Ship Seakeeping Ability, Part 1.* Polish Maritime Research, Vol 8, No.3, September 2001
9. Szelangiewicz T., Cepowski T.: *Application of Artificial Neural Networks to Investigation of Ship Seakeeping Ability, Part 2.* Polish Maritime Research, Vol 8, No.4, December 2001
10. Zhou, Z., Zhou, D., Xie, N: *A Seakeeping Experiment Research on Flokstra Container Ship Model*. Technical Report 4 of Study on Reviewing Freeboards of ICLL 1966. China Classification Society, Shanhai Rules and Research Institute Shanhai. China. 1996

CONTACT WITH THE AUTHOR

Tomasz Cepowski, D.Sc., Eng.
Institute of Marine Navigation,
Maritime University of Szczecin
Wały Chrobrego 1/2
70-500 Szczecin, POLAND
e-mail : cepowski@am.szczecin.pl

FOREIGN conference

Task force 2 workshop of European Federation of Corrosion (EFC)

Under auspices of EFC technical scientific projects are carried out as the task force 2 dealing with :

Corrosion and protection of steel structures against corrosion

The activity is supervised by Prof. K. Darowicki, Head of the Department of Electrochemistry, Corrosion and Materials Engineering, Chemical Faculty, Gdańsk University of Technology.

On 20-21 June 2004 in Prague, the Department in cooperation with the Department of Metals and Corrosion Engineering, Czech's Institute of Chemical Technology, organized the workshop on :

Industrial heat exchanger problems – – Non-destructive Testing (NDT) inspection

Results of altogether 17 projects were presented, 12 out of which were prepared by scientific workers from Gdańsk University of Technology. It was the following presentations :

- Darowicki K., Felisiak W.: *Applications of ellipsometry in corrosion measurements*
- Darowicki K., Kawula J.: *Applications of conducting polymers to corrosion protection – a review*
- Darowicki K., Mirakowski A.: *Use of acoustic emission to detect the pitting corrosion of aluminum*
- Darowicki K., Orlikowski J., Arutunow A.: *Detailed analysis of the passive-active transition during the passive layer cracking using dynamic electrochemical impedance spectroscopy*
- Darowicki K, Ślepski P.: *Electrode impedance measurement of non-stationary systems*
- Darowicki K., Szociński M.: *Impedance investigation of organic coatings subjected to alternating mechanical stress impact*
- Darowicki K., Zieliński A.: *Application of electrochemical noise technique in corrosion monitoring*
- Klenowicz Z., Darowicki K., Krakowiak S., Krakowiak A.: *Flow monitoring shows the way to diminish erosion of tube outer surfaces*
- Krakowiak S., Darowicki K., Ślepski P.: *Pitting corrosion – practical experience and laboratory investigations*
- Miszczyk A., Darowicki K.: *Intercoat adhesion monitoring using impedance spectroscopy*
- Orlikowski J., Krakowiak S., Ślepski P., Darowicki K., Arutunow A.: *Digital monitoring system of corrosion in electrochemical environments*
- Żakowski K.: *A time-frequency method for detection of electromagnetic field interference on metal constructions*.

Apart from the above, 4 reports were presented by scientists from Chech Republic and one from Portugal.

Influence of running ship diesel engines on mixtures of fuel oil and rape oil methyl esters – – experimental tests

Jacek Krzyżanowski
Kazimierz Witkowski
Gdynia Maritime University

ABSTRACT

The paper presents results of experimental tests being continuation of the research project described in the preliminary report [4]. The tests were carried out on a ship diesel engine supplied with marine diesel oil, and the oil and rape oil methyl esters mixed in different proportions. In the tests special attention was paid to influence of combustion of the mixtures on exhaust gas content, including its noxious components, as well as on possible changes of indicated working parameters of the engine.

Keywords : tests, ship engines, renewable fuels, alternative fuels, ecology

INTRODUCTION

In [4] the authors presented an analysis of possible application of alternative fuels to ship diesel engines. As it results from the subject-matter literature on the state of research in this area, for diesel engines possible application of mixtures of diesel oil and vegetable oil esters is most seriously considered. In European conditions it first of all concerns the mixture containing from a few to a dozen or so percent of rape oil esters (RME). Though many tests have been performed, their results are often contradictory, as they have been carried out in very different conditions (different types of diesel engines tested under different loading). Therefore has been emphasized necessity of carrying out tests under constant rotational speed. Simultaneously no report concerning application of alternative fuels in question to ship diesel engines can be found. For this reason the authors were encouraged to undertake the laboratory tests satisfying the above mentioned premises.

LABORATORY TESTS

Object of tests

The tests were carried out with the use of the one-cylinder, two-stroke, crosshead supercharged diesel engine which is an element of the test stand already used for the previous investigations on emission of exhaust gas noxious components, presented by the authors in [1, 2, 3].

The test stand makes it possible to load the engine both with torque and rotational speed. During operation of the engine its most important working parameters, including those electronically indicated, can be recorded. An applied analyzer allows to investigate exhaust gas content.

To supply the engine during the tests in question the marine diesel oil (**MDO**) and its mixtures with rape oil esters (**RME**) of the following proportions, were prepared :

- 5% of RME in MDO
- 10% of RME in MDO.

The MDO was of the density of 831 kg/m^3, and the RME of 883 kg/m^3. As a result of the mixing the biofuel of the density of : 833 kg/m^3 in the first case, and of 836 kg/m^3 in the second case, was obtained. Detail properties of the marine diesel oil and the above specified mixtures were given in [4].

Test program

The tests were carried out within the broad range of engine's loading, namely : at 25, 40, 50, 60, 70, 80 % M/M_r , and for constant rotational speed of the engine, set twofold : at 220 rpm and 320 rpm.

At a given rotational speed and successively set loads, were realized measurements of the engine's working parameters and its exhaust gas content during combusting by the engine : the MDO alone, and the two above specified mixtures (i.e. 5 % RME in MDO, and 10 % RME in MDO).

The results obtained from the tests when supplying the engine with the MDO alone was assumed the reference point for determination of influence of combustion of the MDO/RME mixtures on the engine's working parameters and its exhaust gas content.

Test results and their analysis

The test results are presented in Tab.1 and 2, and the changes of values of selected working parameters of the engine, and of exhaust gas content are graphically shown in Fig.1÷10

Tab. 1. *Test results – exhaust gas content and values of selected working parameters of the engine in function of loading level and kind of fuel, at the constant engine speed of **220** rpm*

Kind of fuel	Loading level	Content of exhaust gas					Values of selected engine working parameters				
	M/M_r	O_2	CO	NO_x		CO_2	p_i	p_{max}	αp_{max}	$p_{max.\,in}$	f_e
	%	ppm	ppm	ppm	mg	%	MPa	MPa	°CSR	MPa	g/kWh
MDO	25	18.5	150	185	254	1.8	0.207	4.32	5.0	26.6	400
	40	18.4	145	273	375	1.8	0.264	4.68	4.5	27.8	316
	50	17.7	156	338	464	2.4	0.309	4.98	6.0	28.5	299
	60	16.7	198	515	707	3.1	0.352	5.34	6.5	32.1	291
	70	14.4	257	793	1035	4.8	0.407	5.57	6.0	28.5	291
	80	12.4	257	1089	1422	6.3	0.441	5.73	5.0	28.8	285
MDO +5 % RME	25	18.4	164	194	266	1.8	0.223	4.29	4.5	27.0	410
	40	18.2	123	244	335	2.0	0.262	4.57	5.0	29.4	326
	50	17.8	176	328	450	2.3	0.303	4.90	6.0	28.2	305
	60	16.4	221	483	663	3.3	0.355	4.87	6.3	32.1	300
	70	14.2	208	759	1042	4.9	0.386	5.39	6.0	28.4	292
	80	12.2	237	1005	1380	6.4	0.451	5.60	6.0	28.2	290
MDO +10 % RME	25	18.4	186	178	244	1.8	0.193	4.18	5.0	26.6	392
	40	18.5	119	226	310	1.8	0.255	4.51	7.0	28.2	314
	50	17.8	170	318	436	2.3	0.314	5.22	7.0	29.1	310
	60	16.8	168	454	623	3.0	0.341	5.20	6.0	30.0	298
	70	14.9	186	689	946	4.4	0.391	5.39	6.0	28.5	290
	80	11.9	280	1009	1386	6.6	0.439	5.56	6.0	28.4	293

Tab.2. *Test results – exhaust gas content and values of selected working parameters of the engine in function of loading level and kind of fuel, at the constant engine speed of **320** rpm*

Kind of fuel	Loading level	Content of exhaust gas					Values of selected engine working parameters				
	M/M_r	O_2	CO	NO_x		CO_2	p_i	p_{max}	αp_{max}	$p_{max.\,in}$	f_e
	%	ppm	ppm	ppm	mg	%	MPa	MPa	°CSR	MPa	g/kWh
MDO	25	17.4	141	288	395	2.6	0.224	4.29	4.5	32.8	384
	40	17.4	121	305	419	2.6	0.284	4.57	6.0	32.6	297
	50	17.7	122	298	409	2.4	0.340	4.82	6.0	32.8	289
	60	17.7	152	341	468	2.4	0.376	5.03	6.5	33.7	278
	70	16.9	196	441	605	2.9	0.417	5.29	7.5	37.4	270
	80	14.8	223	667	916	4.5	0.470	5.46	7.5	38.4	269
MDO +5 % RME	25	17.3	112	313	430	2.7	0.221	4.14	6.8	32.4	392
	40	17.5	162	288	395	2.5	0.278	4.55	6.7	32.3	314
	50	17.8	182	280	384	2.3	0.320	4.71	6.5	31.9	310
	60	17.6	179	314	431	2.4	0.364	4.91	6.8	33.0	298
	70	16.8	154	446	612	3.0	0.406	5.13	6.8	36.6	290
	80	14.7	185	664	912	4.6	0.459	5.32	7.7	37.9	293
MDO +10 % RME	25	17.3	100	303	416	2.7	0.222	4.18	7.0	32.6	370
	40	17.4	138	305	419	2.6	0.267	4.46	6.8	32.6	303
	50	17.9	116	283	388	2.2	0.318	4.70	6.8	32.5	290
	60	17.5	233	336	461	2.5	0.364	4.93	6.8	34.5	286
	70	17.3	143	397	545	2.7	0.403	5.16	7.5	37.2	272
	80	15.6	181	602	827	3.9	0.447	5.29	6.3	38.2	270

for different loads, three kinds of the applied fuels, and a given rotational speed set constant.

Analysis of the results indicates a noticable influence of combustion of the used MDO/RME mixtures on the engine's working parameters and its exhaust gas content against those obtained during combusting the MDO alone.

Within the entire range of the set loads and for both rotational speeds of the engine (220 and 320 rpm) a small drop of the maximum combustion pressure p_{max} , namely by about 3% only (see Fig.1 and 2), can be observed. Simultaneously, a small increase of the respective angle of occurrence of p_{max} , measured from the top dead centre (TDC) of engine's piston, (in Tab.1 and 2 this is the quantity αp_{max}), can be observed. The phenomenon may reveal a somewhat longer time of combustion process of the applied biofuels against that of the MDO alone.

Also, the mean indicated pressure p_i drops to a small degree only. A more distinct drop, by about 3% on average, can be observed during running the engine on the mixture (MDO + + 10%RME) at the engine's speed of 220 rpm, and by about 4% on average at the speed of 320 rpm (see Fig.3 and 4). The small drop of p_i resulted also in a small increase of the specific fuel oil consumption f_e. However in some cases the changes exceeded the measurement error limits only insignificantly.

During the tests the course of pressure in the engine's injection system was recorded. Regardless of a kind of fuel, changes of the pressure for both the engine's speed were small. It is not possible to state a.o. any significant influence of the tested fuels on change of the maximum injection pressure $p_{max,in}$ (see Fig.5 and 6).

On the basis of the exhaust gas analysis it can be stated that combustion of MDO with 5% addition of RME caused on average the drop of NO_x content by over 6%, and that during combusting the MDO with 10% addition of RME the drop on average exceeded 8% (see Fig.7 and 8). However ambiguous are changes of CO content in exhaust gas. As, depending on engine's load, both either a distinct increase or a drop of CO content in exhaust gas, can be observed. For instance, in the case of using both the mixtures at 220 rpm engine speed the drop of CO content in exhaust gas exceeded 15% at the load levels of 40 and 70% M/M_r , but at the load levels of 25, 50, 60 and 80% M/M_r the increase of CO content in exhaust gas by a few to a dozen or so percent see Fig.9 and 10) was observed.

Explanation to Figs 1÷10 :

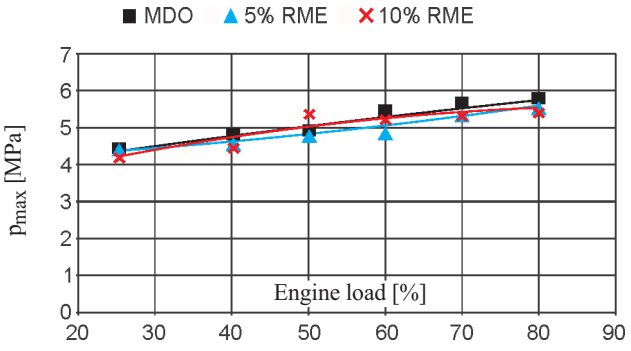

Rys. 1. *Maximum combustion pressure p_{max} in function of engine load for different kinds of fuel at constant engine rotational speed n = **220** obr/min*

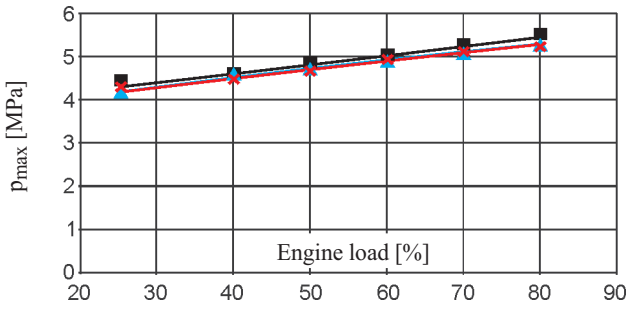

*Rys. 2. Maximum combustion pressure p_{max} in function of engine load for different kinds of fuel at constant engine rotational speed n = **320** obr/min*

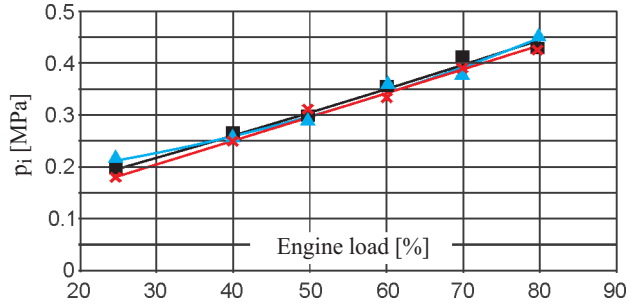

*Rys. 3. Maximum mean indicated pressure p_i in function of engine load for different kinds of fuel at constant engine rotational speed n = **220** obr/min*

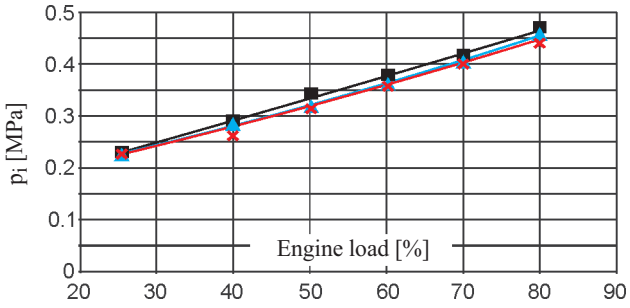

*Rys. 4. Maximum mean indicated pressure p_i in function of engine load for different kinds of fuel at constant engine rotational speed n = **320** obr/min*

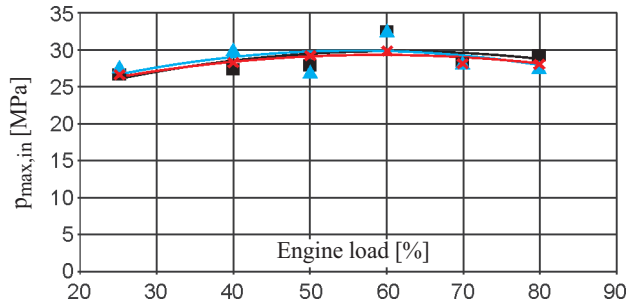

*Rys. 5. Maximum fuel injection pressure $p_{max,in}$ in function of engine load for different kinds of fuel at constant engine rotational speed n = **220** obr/min*

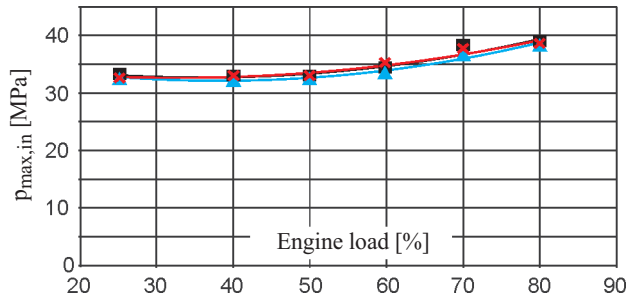

*Rys. 6. Maximum fuel injection pressure $p_{max,in}$ in function of engine load for different kinds of fuel at constant engine rotational speed n = **320** obr/min*

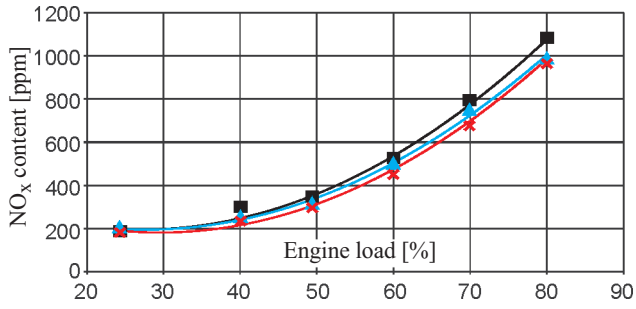

*Rys. 7. NO_x content in exhaust gas in function of engine load for different kinds of fuel at constant engine rotational speed n = **220** obr/min*

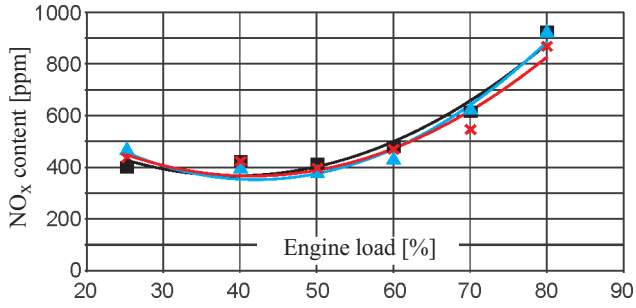

*Rys. 8. NO_x content in exhaust gas in function of engine load for different kinds of fuel at constant engine rotational speed n = **320** obr/min*

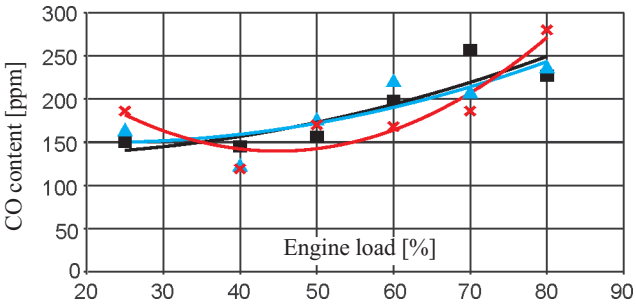

*Rys. 9. CO content in exhaust gas in function of engine load for different kinds of fuel at constant engine rotational speed n = **220** obr/min*

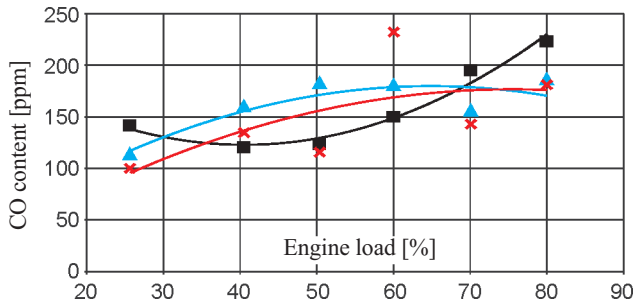

*Rys. 10. CO content in exhaust gas in function of engine load for different kinds of fuel at constant engine rotational speed n = **320** obr/min*

CONCLUSIONS

❖ Running the engine on the MDO/RME mixture made the pressures p_{max} and p_i dropping – especially when using MDO/10% RME fuel – at simultaneous maintaining the engine's speed and torque load constant. It shows that combustion of the fuel proceeded mildly. Most probably, the combustion proceeded more orderly and less dynamically than in the case of combustion of MDO alone. It can be explained by the greater cetan number of RME relative to that of MDO. The increase of cetan number makes the ignition-lag shorter and the work of the engine „soft" , i.e. at

a more moderate increase of combustion pressure. The described probable course of combustion process led to only a small rise of specific fuel consumption.

- The observed , however small, drop of NO_x content seems to confirm the thesis on a more moderate course of combustion process of the fuels containing esters. It may go to show that the maximum combustion temperature was somewhat lower.
- The ambiguous changes of CO content in exhaust gas are difficult to explain in the present phase of the research. It is known that the excess air factor of diesel engines highly varies along with engine's loading. It is favourable that for MDO/RME mixtures CO content in exhaust gas significantly drops at high engine's loads : namely at n = 220 rpm it starts to occur beginning from 75%, and at n = 320 rpm from 70% rated load. It goes to show that the loss due to incomplete combustion appears lower, which indirectly confirms the above formulated theses. This is especially important for ship diesel engines which usually operate under 80÷100% rated load.
- Lack of important differences between values of the maximum fuel injection pressures should be justifed positively, as it shows that a little greater viscosity of RME against that of MDO does not detrimentally influence operation of fuel injectors.
- In the light of the above presented analysis and resulting conclusions it seems reasonable to continue the tests with the MDO/RME mixtures which would have even greater content of the esters.

NOMENCLATURE

CO	–	carbon monoxide
CO_2	–	carbon dioxide
° CSR	–	crank angle [deg]
f_e	–	specific fuel consumption
M	–	set torque of engine
M_r	–	rated torque of engine
NO_x	–	nitrogen oxides
O_2	–	oxygen
P_i(MIP)	–	mean indicated pressure
p_{max}	–	maximum combustion pressure
$P_{max,in}$	–	maximum fuel injection pressure
TDC	–	Top Dead Centre of engine piston
$\alpha_{p\ max}$	–	angle of p_{max} occurrence – measured as crank angle relative to TDC

BIBLIOGRAPHY

1. Krzyżanowski J., Witkowski K. : *On possible lowering of the toxicity of exhaust gas from ship diesel engines by changing their control parameters.* Polish Maritime Research, No. 1(19), March 1999
2. Krzyżanowski J., Witkowski K. : *On effectiveness of lowering the toxicity of exhaust gas from a ship diesel engine by simultaneous changing its two control parameters.* Polish Maritime Research, No. 1(23), March 2000
3. Krzyżanowski J., Witkowski K. : *Research on influence of some ship diesel engine malfunctions on its exhaust gas toxicity.* Polish Maritime Research, No. 1(39), March 2004
4. Krzyżanowski J., Witkowski K. : *On possible supplying ship diesel engines with alternative fuels (mixtures of diesel oils and vegetable oils or their esters).* Polish Maritime Research, No. 4(42), December 2004

CONTACT WITH THE AUTHORS

Jacek Krzyżanowski, D.Sc., Eng.
Kazimierz Witkowski, D.Sc., Eng.
Marine Propulsion Plant Department,
Faculty of Mechanical Engineering,
Gdynia Maritime University
Morska 81÷87
81-225 Gdynia, POLAND
e-mail : jacekk@am.gdynia.pl

Conferences

SemEko 2004

For already three years the SemEko scientific meetings have been organized by Prof. L. Piaseczny, Head of Mechanic-Electric Faculty, Polish Naval University, within the frame of activity of Maritime Technology Unit, Section of Transport Means, Transport Committee, Polish Academy of Sciences.

In the last year two seminars of the kind had place during which the following papers were presented :

- ★ *Camless electro-magnetic timing gear for four-stroke combustion engine* – by K. Zbierski (Łódź University of Technology)
- ★ *Optimization problems of control of piston combustion engines* – by Z. Chłopek (Warsaw University of Technology)

and two papers prepared by J. Pielecha (Poznań University of Technology) :

- ★ *Investigations of emission of noxious components contained in exhaust gas during starting the engine*
- ★ *On possible lowering NO_x emission from diesel engines*.

Conference

ZTM Closing the 2004-year activity

On 4 November 2004 members of the Marine Technology Unit (acting within the Transport Technical Means Section, Transport Committee, Polish Academy of Sciences) met in Maritime University of Szczecin to held its plenary scientific session.

During the scientific part of the meeting two papers were presented :

- ✸ *Ship routing on oceans* – by B.Wiśniewski (Maritime University of Szczecin)
- ✸ *Ultimate strength analysis of ship hull* – by M.Taczała (Technical University of Szczecin)

After discussion on the presented papers the Unit's members adopted the report on the Unit's activity in 2004, presented by Prof. Jerzy Girtler (Gdańsk University of Technology), the Chairman of the Unit, as well as some proposals to the program of the Unit's activities in 2005 were submitted.